Article

Neuron

Altered Cortical Dynamics and Cognitive Function upon Haploinsufficiency of the Autism-Linked Excitatory Synaptic Suppressor MDGA2

Highlights

- Autism-linked *MDGA2* negatively regulates the *NLGN-NRXN* synaptic pathway
- *Mdga2*$^{+/-}$ mice show increased excitatory synapse number and function and altered LTP
- *Mdga2*$^{+/-}$ mice represent a heterozygous model with an autism-like behavior phenotype
- In vivo imaging reveals enhanced activity and hyperconnectivity in *Mdga2*$^{+/-}$ cortex

Authors

Steven A. Connor, Ina Ammendrup-Johnsen, Allen W. Chan, ..., Yu Tian Wang, Tohru Yamamoto, Ann Marie Craig

Correspondence

ytwang@brain.ubc.ca (Y.T.W.), tohru@med.kagawa-u.ac.jp (T.Y.), acraig@mail.ubc.ca (A.M.C.)

In Brief

MDGA2 is genetically linked to autism spectrum disorders (ASDs) and was thought to regulate inhibitory synapse development. Connor et al. show that haploinsufficiency of MDGA2 alters neuroligin-1 signaling and results in increased excitatory synaptic drive, enhanced cortical network dynamics, and impaired cognitive and social function, paralleling phenotypes observed in ASD.

Connor et al., 2016, Neuron *91*, 1052–1068
September 7, 2016
http://dx.doi.org/10.1016/j.neuron.2016.08.016

CellPress

CellPress

Neuron
Article

Altered Cortical Dynamics and Cognitive Function upon Haploinsufficiency of the Autism-Linked Excitatory Synaptic Suppressor MDGA2

Steven A. Connor,[1,2,9] Ina Ammendrup-Johnsen,[1,9] Allen W. Chan,[1,2,9] Yasushi Kishimoto,[3,9] Chiaki Murayama,[4,5] Naokazu Kurihara,[3] Atsushi Tada,[3] Yuan Ge,[1] Hong Lu,[1] Ryan Yan,[1] Jeffrey M. LeDue,[1] Hirotaka Matsumoto,[5] Hiroshi Kiyonari,[6,7] Yutaka Kirino,[3] Fumio Matsuzaki,[8] Toshiharu Suzuki,[5] Timothy H. Murphy,[1] Yu Tian Wang,[2,*] Tohru Yamamoto,[4,*] and Ann Marie Craig[1,*]

[1]Brain Research Centre and Department of Psychiatry
[2]Brain Research Centre and Department of Medicine
University of British Columbia, Vancouver, BC V6T 2B5, Canada
[3]Department of Neurobiophysics, Kagawa School of Pharmaceutical Sciences, Tokushima Bunri University, Sanuki, Kagawa 769-2101, Japan
[4]Department of Molecular Neurobiology, Faculty of Medicine, Kagawa University, Miki-cho, Kagawa 761-0793, Japan
[5]Laboratory of Neuroscience, Faculty of Pharmaceutical Sciences, Hokkaido University, Sapporo, Hokkaido 060-0812, Japan
[6]Animal Resource Development Unit
[7]Genetic Engineering Team
[8]Laboratory for Cell Asymmetry
RIKEN Center for Developmental Biology, Kobe, Hyogo 650-0047, Japan
[9]Co-first author
*Correspondence: ytwang@brain.ubc.ca (Y.T.W.), tohru@med.kagawa-u.ac.jp (T.Y.), acraig@mail.ubc.ca (A.M.C.)
http://dx.doi.org/10.1016/j.neuron.2016.08.016

SUMMARY

Mutations in a synaptic organizing pathway contribute to autism. Autism-associated mutations in *MDGA2* (MAM domain containing glycosylphosphatidylinositol anchor 2) are thought to reduce excitatory/inhibitory transmission. However, we show that mutation of *Mdga2* elevates excitatory transmission, and that MDGA2 blocks neuroligin-1 interaction with neurexins and suppresses excitatory synapse development. *Mdga2*$^{+/-}$ mice, modeling autism mutations, demonstrated increased asymmetric synapse density, mEPSC frequency and amplitude, and altered LTP, with no change in measures of inhibitory synapses. Behavioral assays revealed an autism-like phenotype including stereotypy, aberrant social interactions, and impaired memory. In vivo voltage-sensitive dye imaging, facilitating comparison with fMRI studies in autism, revealed widespread increases in cortical spontaneous activity and intracortical functional connectivity. These results suggest that mutations in *MDGA2* contribute to altered cortical processing through the dual disadvantages of elevated excitation and hyperconnectivity, and indicate that perturbations of the *NRXN-NLGN* pathway in either direction from the norm increase risk for autism.

INTRODUCTION

Autism spectrum disorders (ASDs) are neurodevelopmental disorders characterized by reduced social interaction and communication, increased repetitive behaviors, and altered cognition. Although there is considerable phenotypic and genetic heterogeneity, a major underlying pathway has emerged affecting synaptic transmission (Bourgeron, 2015; Chen et al., 2015). A prominent theory is that ASD is associated with an imbalance in excitatory/inhibitory (E/I) transmission beyond the capacity of neurons to regulate synaptic homeostasis (Nelson and Valakh, 2015; Rubenstein and Merzenich, 2003). Elevated E/I ratio, as originally proposed, is consistent with the high incidence of epilepsy in ASD, on the order of 20% (Amiet et al., 2008). Furthermore, elevation of E/I ratio by optogenetic stimulation of mouse prefrontal cortical pyramidal neurons impaired social interaction behavior (Yizhar et al., 2011).

Yet most mouse models based on a direct synaptic pathway in ASD exhibit a reduced E/I ratio. This direct synaptic pathway involves two of the genes most strongly linked to non-syndromic ASD, *NRXN1* and *SHANK3*, accounting for perhaps 0.2%–1% of cases, as well as *NRXN2*,*3*; *SHANK1*,*2*; *NLGN1*,*3*,*4X*; *DLG4*; and *DLGAP2* (Béna et al., 2013; Glessner et al., 2009; Leblond et al., 2014; Peça and Feng, 2012). These genes encode a pathway acting in synapse development and organization: presynaptic neurexins (Nrxs) bind postsynaptic neuroligins (NLs) which link sequentially to scaffolding proteins of the DLG/MAGUK, DLGAP/SAPAP and SHANK families at excitatory synapses. Related targeted deletions in mice, for example in *Nrxn* or *Shank* genes, reduced excitatory transmission in cortex, hippocampus, and/or striatum, and resulted in behavioral deficits in

social interaction, nest building, learning and memory, and/or enhanced repetitive grooming (Etherton et al., 2009; Jiang and Ehlers, 2013).

We studied a recently identified gene in this synaptic pathway, *MDGA2*, in which protein-truncating loss-of-function mutations were found in ten unrelated ASD cases and no controls, a significant association (Bucan et al., 2009). MDGA2 is highly conserved, 99% identical in humans and mice. MDGA2 and the related MDGA1 are cell-surface proteins that directly bind the inhibitory synapse-selective NL, NL2 (Pettem et al., 2013b). MDGA1, through blocking NL2 interaction with Nrx, selectively suppresses inhibitory synapse development without affecting excitatory synapses in cultured neurons (Pettem et al., 2013b). MDGA2 is also reported to selectively suppress inhibitory and not excitatory synapse development (Lee et al., 2013). Based on these studies, we hypothesized that targeted deletion of *Mdga2* in mice would enhance inhibitory synaptic function and thus reduce E/I ratio, similar to loss of most other genes in the *NRXN-NLGN* synaptic pathway.

Contrary to expectations, we report here that MDGA2 blocks interaction of NL1with Nrx and suppresses excitatory synapse development. Furthermore, targeted deletion of *Mdga2* in mice, even loss of one allele modeling ASD, elevates E/I ratio and enhances resting-state cortical activity and intrahemispheric functional connectivity. Associated behaviors include stereotypy, aberrant social interactions, and impaired cognition. These data suggest that *Mdga2* haploinsufficiency, through disruption of synaptic interactions, elevates both excitatory transmission and functional connectivity to produce behavioral phenotypes related to ASD.

RESULTS

MDGA2 Suppresses the Synaptogenic Function of NL1 and NL2

To assess physical and functional interaction of MDGA2 with the main excitatory neuroligin NL1 or the main inhibitory neuroligin NL2 (Krueger et al., 2012), we performed co-immunoprecipitation assays. Whereas CFP-tagged NL2 selectively co-precipitated with HA-MDGA1, as expected (Pettem et al., 2013b), both NL1 and NL2 co-precipitated with HA-MDGA2 (Figure 1A). Consistently, HA-MDGA2 co-precipitated with both CFP-NL1 and CFP-NL2 (Figure S1A, available online). To determine if MDGA2 suppresses NL-mediated synapse development, we used a co-culture assay in which NLs expressed on non-neuronal cells induce presynaptic differentiation in contacting axons. In comparison with an unrelated negative control membrane protein HA-CD4, co-expression of HA-MDGA2 along with CFP-NL1 or CFP-NL2 significantly suppressed presynaptic induction by either NL1 or NL2 (Figures 1B–1E). In the same assay, HA-MDGA1 suppressed presynaptic induction by NL2, but not NL1, as expected (Pettem et al., 2013b).

Binding of MDGA2 to NLs might inhibit presynapse formation through reducing surface expression of NLs. However, in these co-culture assays, we found no difference in surface levels of CFP-NL1 or CFP-NL2 between cells co-expressing HA-MDGA2 or HA-CD4 control (Figure S1B). Alternatively, MDGA2 might suppress synaptogenesis by inhibiting trans-synaptic interaction between NLs and presynaptic Nrxs. To test this idea, we performed a cell-based binding assay with a Myc-tagged soluble ectodomain of Nrx-1β fused to alkaline phosphatase (Myc-Nrx-AP). In comparison with HA-CD4 control, cells co-expressing HA-MDGA2 together with CFP-NL1 or CFP-NL2 showed significantly reduced binding of Myc-Nrx-AP (Figures 1F–1I). These data indicate that, similar to MDGA1, MDGA2 restricts presynaptic induction through postsynaptic interaction with NL and inhibition of NL interaction with Nrxs. However, counter to our initial hypothesis, MDGA2 binds and negatively regulates the synaptogenic function of NL1 as well as NL2.

Overexpression of MDGA2 Suppresses Synapse Development in Cultured Neurons

Given our data suggesting that MDGA2 prevents the synapse promoting NL-Nrx interaction, we hypothesized that overexpression of MDGA2 would reduce synapse development in neurons. To assay this, we compared synapse density in cultured neurons transfected with either HA-MDGA2 or control V5-CD4 (Figures 2A–2D). Quantification of clusters of presynaptic vesicular GABA transporter (VGAT) apposed to gephyrin postsynaptic scaffolds revealed reduced density of inhibitory synapses. Excitatory synapse density was similarly suppressed as shown by reduced vesicular glutamate transporter (VGluT1)-positive PSD-95 clusters in neurons overexpressing HA-MDGA2. To determine if MDGA2 overexpression resulted in reduction of functional indicators of synapse density, we quantified miniature inhibitory and excitatory postsynaptic currents (mIPSCs and mEPSCs). Both mIPSC and mEPSC frequencies were significantly reduced in neurons overexpressing MDGA2 relative to control CD4, with no change in respective amplitudes (Figures 2E–2J). These data indicate that excess MDGA2 limits excitatory and inhibitory synapse development in cultured neurons.

MDGA2 Is Highly Expressed in Neocortex and Hippocampus and Knockout Is Lethal

To determine if MDGA2 suppresses synapse development in vivo, we generated *Mdga2* knockout mice (Figure S2). Reduction of MDGA2 protein in $Mdga2^{+/-}$ mice and loss in $Mdga2^{-/-}$ mice were confirmed by western blotting (Figure S2C). Second filial generation (F2) $Mdga2^{-/-}$ mice were born at a normal Mendelian rate (wild-type [WT]:+/−:−/− = 28:51:36). However, although lacking gross anatomical brain defects (Figure S2D), two-thirds of F2 $Mdga2^{-/-}$ mice died by postnatal day 10 (P10). Upon further backcrossing to C57BL6, full knockout of *Mdga2* proved to be perinatal lethal (Figure 3A). *Mdga2* heterozygous mice were viable and fertile on a C57BL6 background, with no obvious defects in gross brain morphology into adulthood. Previous data suggested roles for MDGAs in cortical lamination (Ishikawa et al., 2011; Perez-Garcia and O'Leary, 2016; Takeuchi and O'Leary, 2006). Thus, we assessed cortical morphology using Nissl stain and layer-specific markers Cux2 and Er81 but observed no obvious deficits in adult $Mdga2^{+/-}$ mice (Figure S2E).

To choose brain regions for in-depth analysis in *Mdga2* mutant mice, we first assessed the expression pattern of MDGA2. As $Mdga2^{+/-}$ mice were generated by knockin of lacZ (Figure S2A), we used β-galactosidase activity as a sensitive readout of

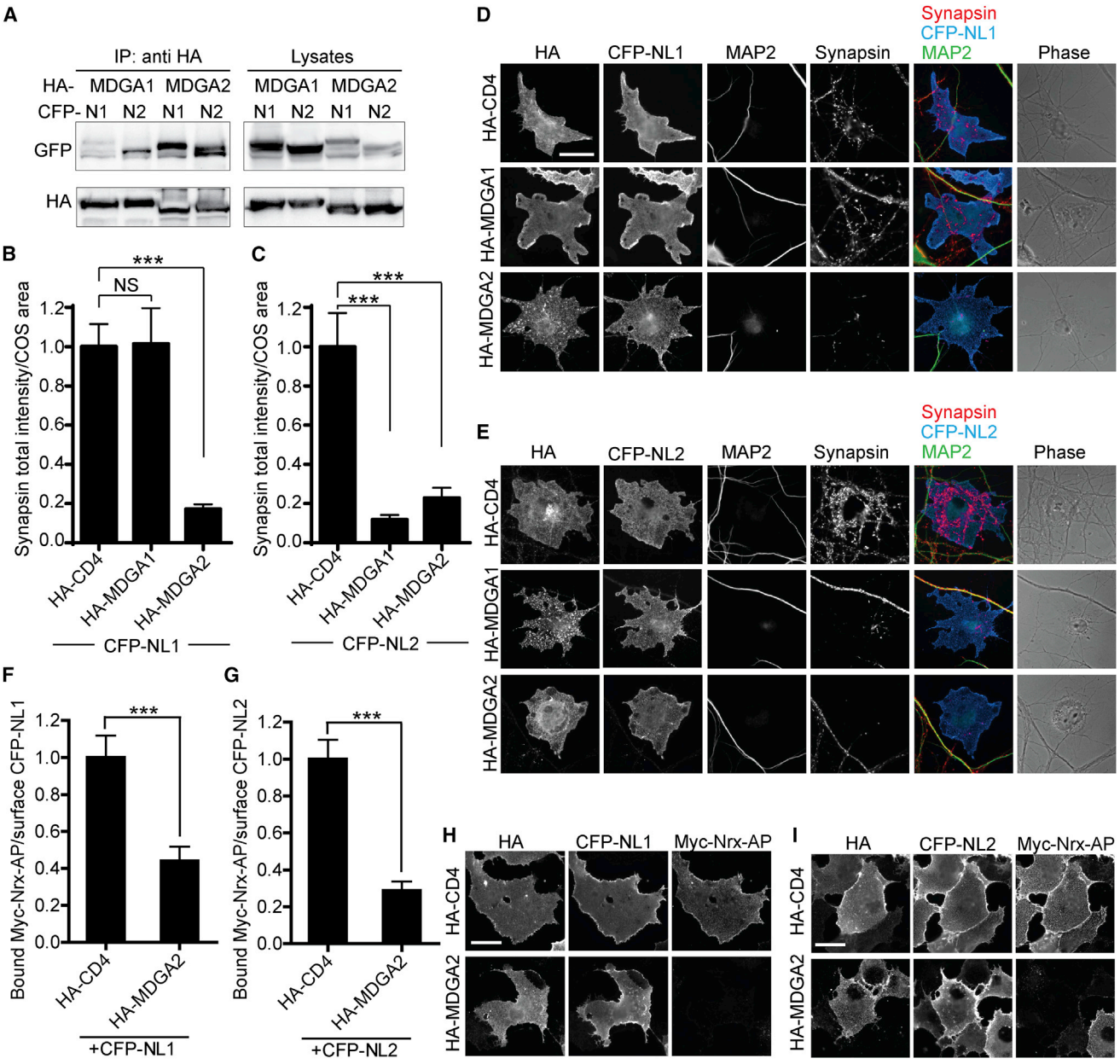

Figure 1. MDGA2 Inhibits the Synaptogenic Activity of NL1 and NL2 by Blocking Their Interaction with Nrx

(A) Recombinant NL1 and NL2 both co-immunoprecipitated (IP) with MDGA2, whereas NL2 selectively co-immunoprecipitated with MDGA1 when co-expressed in HEK293 cells.

(B–E) In the co-culture assay, NLs on COS7 cells co-cultured with hippocampal neurons induce synapsin clustering in contacting axons; induced clusters are differentiated from native synapses by the absence of MAP2-positive dendrites. Co-expression of MDGA2, but not MDGA1 or CD4 control, together with NL1 (B and D) in COS7 cells, suppressed the synapsin clustering induced by NL1 (one-way ANOVA, $F_{2,\ 87} = 14.9$, $p < 0.0001$; ***$p < 0.0001$; or NS, not significant [$p > 0.999$], by Bonferroni's post hoc test; n = 30 cells from 3 independent experiments). In contrast to the differential effect of MDGAs on NL1, synapsin clustering induced by NL2 was suppressed by both MDGA1 and MDGA2 compared to CD4 (C and E; one-way ANOVA, $F_{2,\ 87} = 21.31$, $p < 0.0001$; ***$p < 0.0001$ by Bonferroni's post hoc test; n = 30 cells each). Punctate synapsin intensity associated with COS7 cells expressing both HA and CFP fusion proteins and not associated with MAP2 was measured.

(F–I) Co-expression of MDGA2 compared with control CD4 inhibited the binding of Nrx-1β ectodomain (Myc-Nrx-AP) to NL1 (F and H; unpaired t test, $t_{58} = 3.975$, ***$p = 0.0002$) or NL2 (G and I; unpaired t test, $t_{58} = 6.117$, ***$p < 0.001$) expressed on the surface of COS7 cells (n = 30 cells from 3 independent experiments). Bound Myc-Nrx-AP was measured per surface CFP-NL and the ratio normalized to the average value for cells expressing CFP-NL1 or CFP-NL2 with the CD4 control.

Scale bars, 20 μm. Error bars indicate SEM. See also Figure S1.

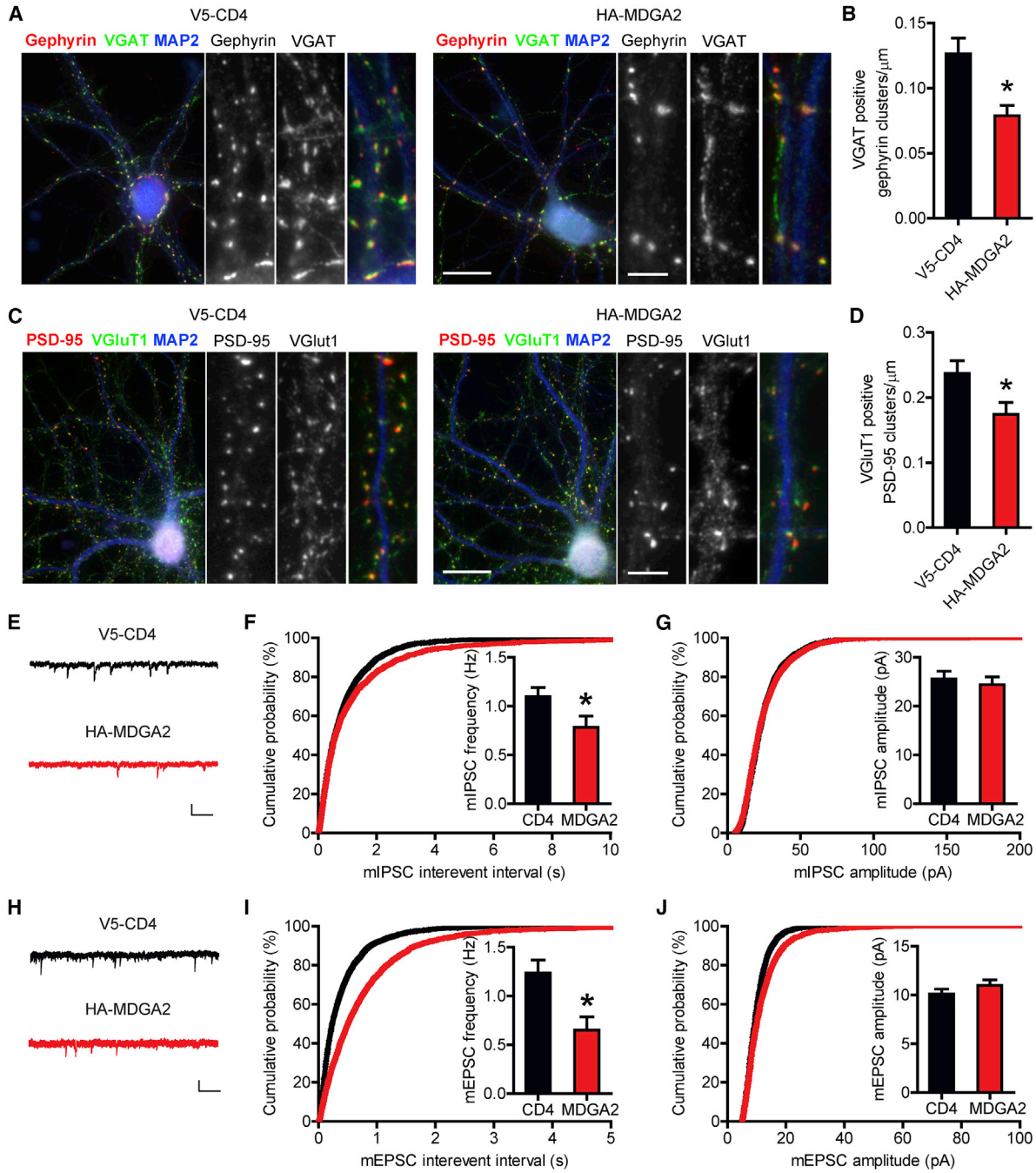

Figure 2. Overexpression of MDGA2 Suppresses Both Inhibitory and Excitatory Synapse Development

Hippocampal neurons were transfected with the indicated constructs at plating and analyzed at 14–17 DIV (days in vitro). For (E)–(J), GFP was co-expressed to mark transfected cells for recording.

(A and B) Overexpression of HA-MDGA2 relative to control V5-CD4 resulted in a reduction in the density of VGAT-positive gephyrin clusters (A, representative images; B, unpaired t test, $t_{49} = 2.370$, *$p < 0.05$, $n \geq 25$ cells from 3 independent experiments). Scale bars, 20 (cells) and 5 μm (dendrites).

(C and D) VGlut1-positive PSD-95 cluster density was similarly reduced by HA-MDGA2 overexpression (C, representative images; D, unpaired t test, $t_{41} = 3.311$, *$p < 0.01$, $n \geq 25$ cells from 3 independent experiments). Scale bars, 20 (cells) and 5 μm (dendrites).

(E–G) mIPSC frequency (F) was significantly reduced in HA-MDGA2-expressing neurons (n = 14) relative to cells transfected with V5-CD4 (n = 15; $t_{25} = 2.138$, *$p < 0.05$). There was no change in mIPSC amplitude (G; $p > 0.05$). Sample trace (E) scale bar, 40 pA, 1 s.

(H–J) Overexpression of HA-MDGA2 (n = 15) similarly reduced frequency of mEPSCs relative to V5-CD4 transfected controls (I; n = 16; $t_{28} = 3.111$, *$p < 0.01$) without altering mEPSC amplitude (J; $p > 0.05$). Sample trace (H) scale bar, 20 pA, 1 s.

Error bars indicate SEM.

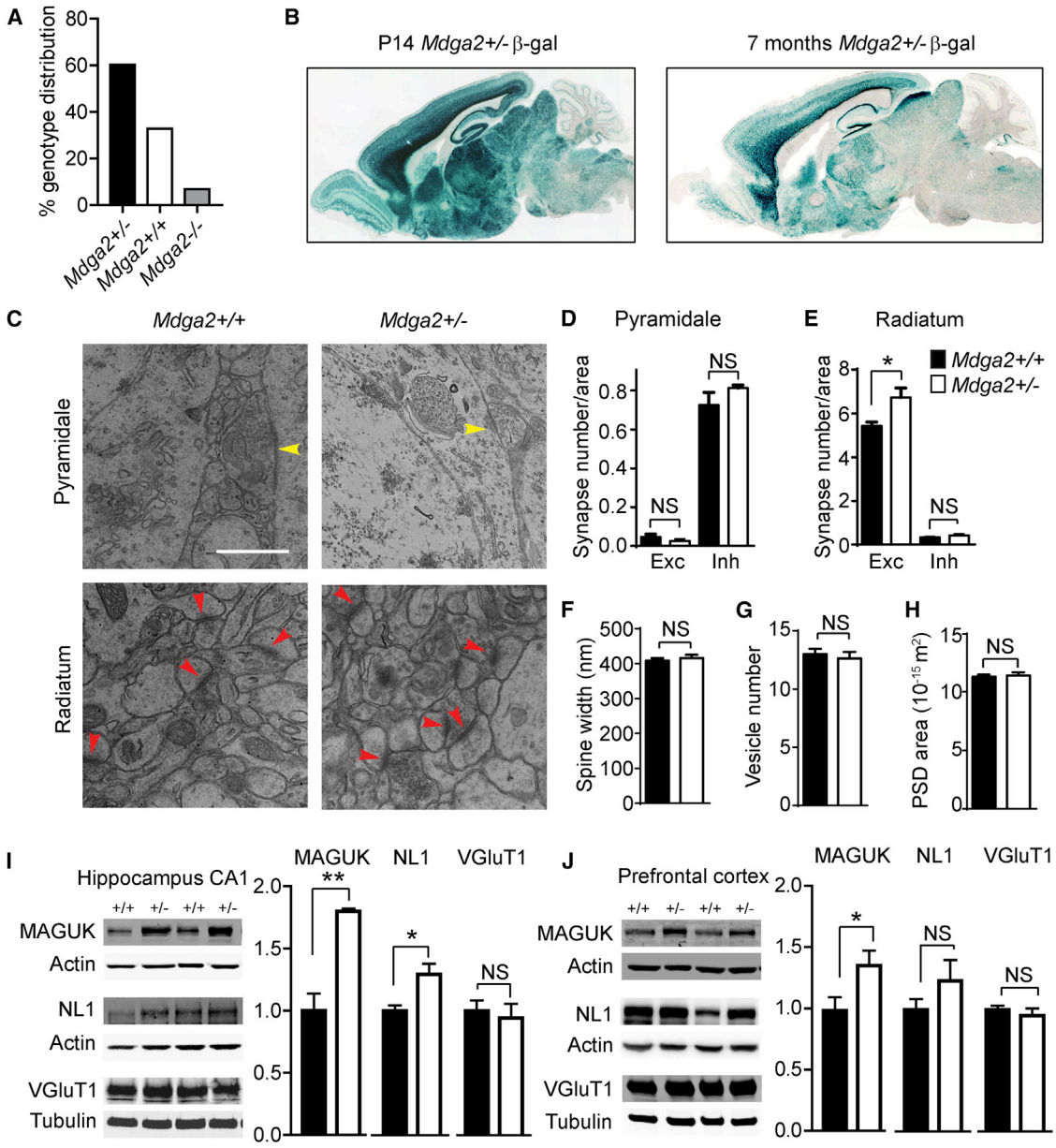

Figure 3. *Mdga2* Knockout Is Lethal and Haploinsufficiency Increases Excitatory Synapse Density

(A) Genotype distribution of P14 pups from *Mdga2*$^{+/-}$ crosses. Few *Mdga2*$^{-/-}$ pups survived and these survivors were runty.

(B) β-galactosidase activity expressed from the *Mdga2* locus is shown with development as a readout of the MDGA2 expression pattern.

(C–E) Asymmetric (red arrow) and symmetric (yellow arrow) synapses are indicated in the representative images from hippocampal CA1 stratum pyramidale and radiatum (C). *Mdga2*$^{+/-}$ mice showed a selective increase in the density of asymmetric synapses (Exc) in stratum radiatum (E) as compared with WT mice (unpaired t test, $t_6 = 2.770$, p = 0.0324) with no difference in the number of symmetric synapses (Inh, $t_6 = 1.285$, p = 0.2461). Stratum pyramidale (D) showed no difference in either asymmetric ($t_6 = 1.149$, p = 0.2941) or symmetric ($t_6 = 1.304$, p = 0.2399) synapse density. NS, not significant; n = 4 mice per group. Scale bar, 1 μm.

(F–H) Morphological measures from asymmetric synapses showed no significant difference in spine width (F; unpaired t test, $t_{749} = 0.520$, p = 0.603), synaptic vesicle number per terminal (G; $t_{777} = 0.585$, p = 0.559), or postsynaptic density (PSD) area (H; $t_6 = 0.0596$, p = 0.954) between *Mdga2*$^{+/-}$ and WT mice. NS, not significant.

(I and J) Immunoblots revealed an upregulation of postsynaptic NL1 and PSD-95 family MAGUK proteins in *Mdga2*$^{+/-}$ hippocampal CA1 (I; t tests; MAGUKs, $t_6 = 5.78$, **p = 0.0012; NL1, $t_6 = 3.158$, p = 0.0196), and for MAGUKs in PFC (J; $t_{14} = 2.27$, *p = 0.0395), with no significant change in level of NL1 in PFC ($t_{14} = 1.24$, p = 0.237). Protein levels were normalized to the loading control (β-actin or tubulin) and then normalized to the mean of the WT value. n = 4 (CA1) or 8 (PFC) mice per genotype. NS, not significant.

Error bars indicate SEM. See also Figures S2 and S3.

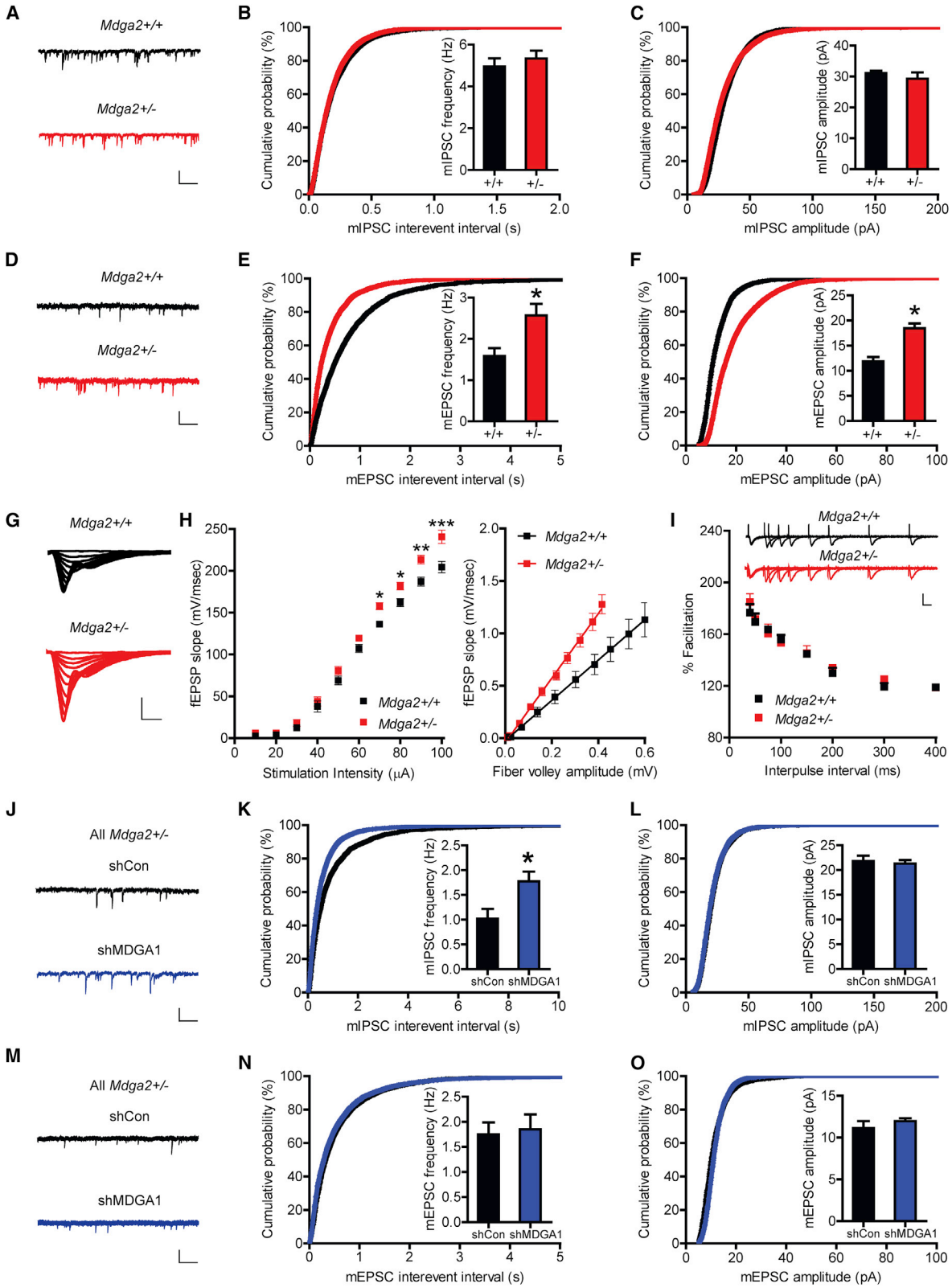

(legend on next page)

MDGA2 expression. At P14, a stage of high expression, β-galactosidase activity staining in *Mdga2*$^{+/-}$ mice reflected reasonably well the expression pattern of native MDGA2 analyzed by in situ hybridization in WT mice (Figure S3A). At P14, MDGA2 expression was high in most forebrain regions, including deep cortical layers, hippocampus, thalamus, and striatum, and detected in midbrain, hindbrain, and cerebellar nuclei and Purkinje cells. MDGA2 expression estimated from β-galactosidase activity appeared to diminish at later stages of development but was still detected in adult mice, particularly in deep cortical layers, anterior olfactory nucleus, superior colliculus, dentate gyrus, and hippocampal CA1 regions (Figure 3B). These expression patterns of MDGA2 are consistent with previous reports (Lee et al., 2013; Litwack et al., 2004). At the cellular level, β-galactosidase immunofluorescence was detected in a subset of pyramidal cells and interneurons in CA1, including parvalbumin-positive interneurons, and a subset of cortical neurons (Figures S3B–S3D). At the subcellular level, recombinant epitope-tagged MDGA2 distributed diffusely in cultured hippocampal neurons with no obvious concentration at excitatory or inhibitory synapses (Figures S3E and S3F).

Excitatory Synapse Density Is Increased in *Mdga2*$^{+/-}$ Mouse Hippocampus

Mdga2$^{+/-}$ mice model the genetic deletions found in a subset of ASD patients (Bucan et al., 2009). Many mouse knockouts in the synaptic pathway in ASD only show phenotypes in homozygous form; however, given the perinatal lethality of *Mdga2*$^{-/-}$ mice, we wondered whether *Mdga2*$^{+/-}$ mice might show altered synapse density, synaptic function, or behavior. As we were interested in persistent changes, all assays described below were performed on adult mice.

Given the persistent expression of MDGA2 in hippocampal CA1 neurons from postnatal to adult stages, we quantified symmetric (inhibitory) and asymmetric (excitatory) synapse number in CA1 stratum pyramidale and stratum radiatum (Figures 3C–3E). *Mdga2*$^{+/-}$ mice showed an increase in asymmetric synapse density in CA1 stratum radiatum relative to WT littermates (24%). No differences were detected in symmetric synapse density in stratum radiatum or in either synapse subtype in stratum pyramidale. Morphological features of spine width, synaptic vesicle number, and postsynaptic density area appeared unchanged in asymmetric synapses of *Mdga2*$^{+/-}$ mice (Figures 3F–3H). These data indicate that MDGA2 negatively regulates excitatory, but not inhibitory, synapse density within the hippocampus.

NL1 and PSD-95 Family MAGUKs Are Elevated in *Mdga2*$^{+/-}$ Mice

Our data suggests that MDGA2 may regulate excitatory synapse numbers by suppressing the function of NL1. We next assessed whether levels of NL1 or associated PSD-95 family MAGUK proteins (Giannone et al., 2013; Irie et al., 1997) are altered following genetic reduction of MDGA2. Quantitative immunoblotting of microdissected CA1 and prefrontal cortex (PFC) tissue was performed. The levels of PSD-95 family MAGUKs were significantly elevated in *Mdga2*$^{+/-}$ CA1 and PFC relative to WT littermates (Figures 3I and 3J). NL1 level was increased in CA1, with a non-significant trend toward increased levels in PFC. No changes were observed in levels of NL2 or the inhibitory scaffold protein gephyrin, nor of presynaptic transporters VGluT1 or VGAT (Figures 3I, 3J, and S3G). Thus, haploinsufficiency of *Mdga2* results in a specific upregulation of some excitatory postsynaptic proteins.

Excitatory, but Not Inhibitory, Synaptic Transmission Is Enhanced in *Mdga2*$^{+/-}$ Mouse Hippocampus

To determine if basal synapse function is altered as a result of *Mdga2*$^{+/-}$ haploinsufficiency, we performed whole-cell recordings from CA1 pyramidal cells in hippocampal slices from *Mdga2*$^{+/-}$ and WT littermate mice. No differences were detected in mIPSC frequency or amplitude (Figures 4A–4C). In contrast, mEPSC recordings from *Mdga2*$^{+/-}$ mouse pyramidal neurons showed a 30% increase in mEPSC frequency relative to WT (Figure 4E). The amplitude of mEPSCs was also significantly enhanced (Figure 4F). The observed enhancement in mEPSC frequency is consistent with our ultrastructural data, indicating a function of MDGA2 in suppressing excitatory synapse density.

To test evoked transmission, we generated input/output curves by stimulating Schaffer collateral (SC) axonal fibers while recording field excitatory postsynaptic potentials (fEPSPs) from stratum radiatum in CA1. An input/output curve comparing fEPSP slope to stimulus strength or to presynaptic fiber volley amplitude

Figure 4. Excitatory Synaptic Transmission Is Enhanced, Whereas Inhibitory Transmission Is Still Limited, by MDGA1 in *Mdga2*$^{+/-}$ Neurons

For (A)–(I), synaptic transmission was analyzed in CA1 region of adult mouse hippocampal slices. For (J)–(O), hippocampal neurons were cultured from *Mdga2*$^{+/-}$ mice, transfected at plating with shMDGA1 or shCon plus GFP to mark transfected cells, and analyzed at 15–17 DIV.

(A–C) No significant differences were found between *Mdga2*$^{+/-}$ and WT neurons in mIPSC frequency (B; unpaired t test, $t_{15} = 0.7139$, p = 0.4862) or amplitude (C; $t_9 = 0.8036$, p = 0.4423; n = 8 *Mdga2*$^{+/-}$ and 9 WT cells). Sample trace (A) scale bar, 40 pA, 1 s.

(D–F) mEPSCs from *Mdga2*$^{+/-}$ hippocampal neurons showed increased frequency (E; unpaired t test, $t_{15} = 2.920$, p = 0.0106) and amplitude (F; $t_{16} = 5.102$, p = 0.001) compared with WT (n = 10 *Mdga2*$^{+/-}$ and 9 WT cells). Sample trace (D) scale bar, 20 pA, 1 s.

(G) Representative fEPSPs from CA1 with increasing stimulation intensity (scale bar, 1 mV, 5 ms).

(H) fEPSPs were significantly elevated in *Mdga2*$^{+/-}$ hippocampal slices (two-way repeated-measures ANOVA, $F_{1, 9} = 2.781$, p = 0.0047; *p < 0.05, **p < 0.01, and ***p < 0.001 by Bonferroni's post hoc test; n = 10 *Mdga2*$^{+/-}$ and 8 WT slices). Linear fit slopes comparing fiber volley to fEPSP amplitude plots in *Mdga2*$^{+/-}$ (3.08 ± 0.11) and WT (1.92 ± 0.13) slices were significantly different (p < 0.0001).

(I) Paired-pulse facilitation was not significantly different between groups (two-way repeated-measures ANOVA, $F_{1, 7} = 0.3707$, p = 0.9149; n = 4 slices per group). Scale bar, 1 mV, 20 ms.

(J–L) In *Mdga2*$^{+/-}$ cultured neurons, the frequency of mIPSCs was significantly elevated upon knockdown of MDGA1 (shMDGA1, n = 14) relative to control (shCon, n = 14; K, unpaired t test, $t_{25} = 2.717$, *p < 0.001). Amplitude of mIPSCs was not altered (L; $t_{22} = 0.406$, p = 0.688). Sample trace (J) scale bar, 40 pA, 1 s.

(M–O) In *Mdga2*$^{+/-}$ cultured neurons, mEPSCs were similar in both frequency and amplitude between shMDGA1 (n = 13) and shCon (n = 12) cells (N; unpaired t test, frequency $t_{22} = 0.273$, p = 0.393; O, amplitude $t_{14} = 0.964$, p = 0.351). Sample trace (M) scale bar, 20 pA, 1 s.

Error bars indicate SEM. See also Figure S4.

yielded significantly higher fEPSP responses in *Mdga2*$^{+/-}$ slices relative to WT controls (at stimulus intensities >70 μA; Figures 4G and 4H). No changes in paired-pulse facilitation (Figure 4I) or readily releasable vesicle pool depletion rates (Figure S4A) were detected at these synapses, consistent with effects on synapse density and postsynaptic properties. However, fEPSP responses during 14 Hz stimulation showed a decrease in amplitude (Figure S4B), which typically reflects increased mobilization of reserve pool vesicles and suggests some alteration in presynaptic function.

In contrast to our cell culture data showing that MDGA2 can suppress inhibitory synapse development (Figure 2), there were no detectable changes in symmetric synapse density (Figures 3C–3E) or basal inhibitory synaptic transmission in *Mdga2*$^{+/-}$ mouse hippocampal slices (Figures 4B and 4C). Previous results demonstrated that MDGA1 selectively suppresses inhibitory synapse development (Pettem et al., 2013b), suggesting that MDGA1 may be partially redundant or able to functionally compensate for loss of MDGA2 with respect to regulating inhibitory synapses. To test this idea, we used short hairpin RNA (shRNA) against MDGA1 (shMDGA1) (Pettem et al., 2013b) to knock down MDGA1 in *Mdga2*$^{+/-}$ neuron cultures. Relative to sister neurons transfected with control shRNA (shCon), *Mdga2*$^{+/-}$ neurons harboring shMDGA1 showed a significant enhancement in mIPSC frequency with no change in amplitude (Figures 4J–4L). MDGA1 knockdown did not alter mEPSC frequency or amplitude (Figures 4M–4O). These data indicate that MDGA1 is sufficient to maintain normal inhibitory, but not excitatory, synapse density when MDGA2 is reduced.

Mdga2 Haploinsufficiency Enhances GluA1 Synaptic Surface Levels and AMPA Receptor-Mediated Transmission and Alters Synaptic Plasticity

In addition to its role in controlling excitatory synapse density, the increase in mEPSC amplitude in *Mdga2*$^{+/-}$ neurons (Figure 4F) suggests that MDGA2 may control additional postsynaptic properties. To probe the basis for such changes, we analyzed GluA1 immunofluorescence in *Mdga2*$^{+/-}$ hippocampal neurons in culture and found the level of synaptic surface GluA1 (mean intensity per synapse) was elevated in *Mdga2*$^{+/-}$ neurons (Figures 5A and 5B). In addition, as expected from the in vivo data, the density of excitatory synapses identified as VGluT1-positive PSD-95 clusters was elevated in *Mdga2*$^{+/-}$ neurons relative to sister WT cells (Figures 5A and 5C). Consistent with the culture data, recordings of CA1 pyramidal neurons with SC stimulation revealed an increase in AMPA to NMDA ratio in *Mdga2*$^{+/-}$ slices compared with WT (Figure 5D). Thus, *Mdga2* haploinsufficiency alters synaptic transmission in multiple ways, increasing functional excitatory synapses, synaptic surface AMPA receptor levels, and AMPA/NMDA ratio.

Given such changes in postsynaptic properties as well as previous data linking NL1 to synaptic plasticity (Blundell et al., 2010; Shipman and Nicoll, 2012), we next assessed long-term potentiation (LTP) in *Mdga2*$^{+/-}$ mice. Application of high-frequency stimulation (1 × 100 Hz, 1 s) to the SC-CA1 pathway induced LTP that was significantly enhanced in *Mdga2*$^{+/-}$ hippocampal slices relative to WT (Figure 5E). In contrast to such early phase LTP (E-LTP), which typically lasts <3 hr, application of multiple trains of stimulation induces a long-lasting form of LTP (L-LTP; Huang and Kandel, 1994; Reymann and Frey, 2007). Application of an L-LTP stimulation paradigm (4 × 100 Hz) resulted in a deficit in LTP maintenance in *Mdga2*$^{+/-}$ hippocampal slices compared to WT controls (Figure 5F). Taken together, these data indicate that AMPA receptor synaptic transmission and E-LTP are enhanced but L-LTP is compromised upon genetic reduction of MDGA2.

Mdga2 Haploinsufficiency Results in Behavioral Phenotypes Related to ASD

We next examined the effect of *Mdga2* haploinsufficiency and associated altered excitatory transmission on behavior. *Mdga2*$^{+/-}$ mice showed generally normal home-cage behavior with a propensity to be slightly active in terms of traveled distance ($p = 0.075$; Figure S5A). However, *Mdga2*$^{+/-}$ mice spent a greater fraction of time than WT mice in jumping (Figure S5A), including more episodes of repetitive jumping behavior rarely exhibited by WT mice (Figure 6A). Such repetitive jumping is considered a motor stereotypy relevant to repetitive behavioral symptoms of ASD (Silverman et al., 2010). General motor coordination of *Mdga2*$^{+/-}$ mice was similar to that of WT littermates in rotarod and fixed bar tests (Figure S5B). Thus, although MDGA2 is expressed by Purkinje cells and cerebellar nuclei (Figures 3B and S3A), MDGA2 dosage reduction did not significantly impair mouse motor activities, but enhanced motor stereotypy.

Along with repetitive behavior, another core symptom of ASD is profound social impairment, including avoidance behaviors (American Psychiatric Association, 2000). Thus, we examined social behavior of *Mdga2*$^{+/-}$ mice. In a social affiliation test, *Mdga2*$^{+/-}$ mice spent significantly less time than WT littermates investigating an unfamiliar mouse in the center of a test field (Figure 6B). This reduced contact does not seem to be due to any difference in physical activity level, since the distance *Mdga2*$^{+/-}$ mice traveled during the test was comparable to that of WT. To confirm the observed social impairment, we exposed mice to a three-chamber task in which the middle chamber is bordered by two chambers, one containing an unfamiliar mouse in a cage and the other a cage only. WT mice spent more time investigating the unfamiliar mouse than the empty cage as expected; however, *Mdga2*$^{+/-}$ mice did not display a preference for interaction with the new mouse (Figure 6C). Thus, overall, *Mdga2*$^{+/-}$ mice exhibited a selective impairment in social interaction. Contrary to the observed unwillingness of *Mdga2*$^{+/-}$ mice to engage other mice, *Mdga2*$^{+/-}$ mice more actively investigated non-living objects than WT littermates (Figure 6D), frequently climbing onto the objects.

Cognitive Performance Is Impaired upon Genetic Reduction of MDGA2

Although ASD can be associated with savant skills, it is more frequently associated with intellectual disability, perhaps reflecting shared risk genes in the synaptic pathway (Bourgeron, 2015). Deficits in L-LTP are also typically associated with memory deficits in mouse models. Thus, we tested *Mdga2*$^{+/-}$ mice in three assays for learning and memory. Given the L-LTP deficit in the SC-CA1 pathway of *Mdga2*$^{+/-}$ mice, we first examined spatial learning and memory using the Morris water maze test (MWM), which requires intact hippocampal CA1 function (Tsien et al.,

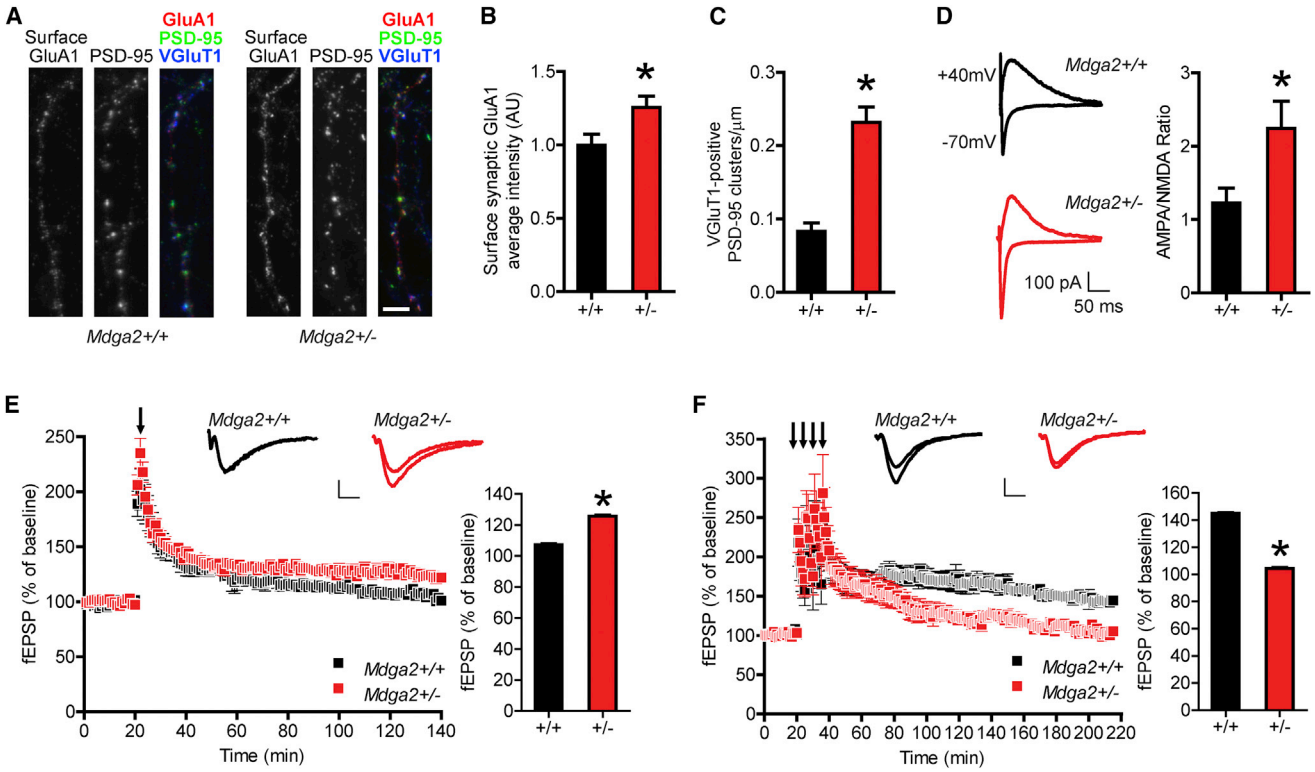

Figure 5. *Mdga2* Haploinsufficiency Elevates Surface Synaptic GluA1 and AMPA Receptor Currents and Alters LTP

(A–C) Hippocampal cultures from *Mdga2*$^{+/-}$ and littermate WT mice were immunolabeled at 22–23 DIV for synaptic markers (A). The mean intensity of surface GluA1 at synaptic sites was elevated in *Mdga2*$^{+/-}$ neurons (B; unpaired t test, $t_{56} = 2.361$, *p = 0.0218; n = 29–30 cells from 2 independent experiments). The density of VGlut1-positive PSD-95 clusters was also increased in *Mdga2*$^{+/-}$ neurons relative to WT (C; unpaired t test, $t_{44} = 6.322$, *p < 0.0001). Scale bar, 5 μm.

(D) AMPA to NMDA ratio was elevated in hippocampal neurons of *Mdga2*$^{+/-}$ mice. Responses were recorded at +40 mV for NMDA and −70 mV for AMPA receptor-mediated currents in WT (n = 14) and *Mdga2*$^{+/-}$ (n = 15) CA1 neurons in adult slices. Comparison of AMPA/NMDA ratio revealed a significant enhancement in *Mdga2*$^{+/-}$ cells ($t_{21} = 2.384$, p = 0.0267; *p < 0.05).

(E) LTP induced by 1 × 100 Hz stimulation (E-LTP) was increased in *Mdga2*$^{+/-}$ slices relative to WT (*Mdga2*$^{+/-}$, 125.6% ± 0.59%; WT, 107.2% ± 0.56%; unpaired t test, $t_{37} = 22.28$, *p < 0.0001; n = 10 *Mdga2*$^{+/-}$and 8 WT slices). Inset: traces taken at 10 min pre- and 120 min post-tetanization (scale bar, 1 mV, 5 ms). Bar graph: fEPSPs compared 100 to 120 min post-tetanization.

(F) LTP induced by 4 × 100 Hz stimuli applied 5 min apart (L-LTP) was impaired in *Mdga2*$^{+/-}$ slices (*Mdga2*$^{+/-}$, 104.3% ± 0.76%; WT, 145.0% ± 0.55%, unpaired t test, $t_{38} = 43.29$, *p < 0.0001; n = 6 slices per group). Inset: traces taken at 10 min pre- and 170 min post-L-LTP induction (scale bar, 1 mV, 5 ms). Bar graph: fEPSPs compared during the last 20 min of recording.

Error bars indicate SEM.

1996). *Mdga2*$^{+/-}$ mice could swim and willingly found a visible platform as well as WT littermates, but failed to reduce the time to reach a hidden platform even after consecutive trials (Figure 6E). A probe trial similarly revealed an impairment for escape platform location in *Mdga2*$^{+/-}$ mice. These observations suggested that *Mdga2*$^{+/-}$ mice suffer from hippocampus-dependent spatial learning and memory deficits.

We examined another hippocampus-dependent learning and memory task, contextual fear conditioning (Lee and Kesner, 2004). *Mdga2*$^{+/-}$ mice could learn to associate the conditioning chamber with a footshock and exhibited nearly comparable contextual memory as WT mice at 1 hr after training (Figure 6F). However, consistent with the MWM results, *Mdga2*$^{+/-}$ mice demonstrated impaired contextual memory performance at 24 hr and 7 days following training.

We further examined the cognitive impairment of *Mdga2*$^{+/-}$ mice using a simpler and less stressful task, novel object recognition. Although this is a non-spatial task, under the conditions used here (≥30 min delay between sample and test sessions), it is also thought to depend significantly on hippocampal function (Cohen and Stackman, 2015). *Mdga2*$^{+/-}$ mice were attracted more strongly to the objects placed in the test cage than WT littermates (Figure 6D); however, unlike WT mice, *Mdga2*$^{+/-}$ mice did not show a preference for a novel object over a familiar object (Figures 6G and S6). Taken together, these data suggest that *Mdga2*$^{+/-}$ haploinsufficiency compromises cognitive performance in tasks requiring hippocampal function, increases the frequency of a motor stereotypy, and impairs social interactions.

Resting-State Cortical Activity and Intrahemispheric Functional Connectivity Are Enhanced in *Mdga2*$^{+/-}$ Mice

In addition to hippocampus, MDGA2 expression is prominent in cortex of adult mice (Figure 3B). To assess the effect of *Mdga2* haploinsufficiency on cortical function across many regions,

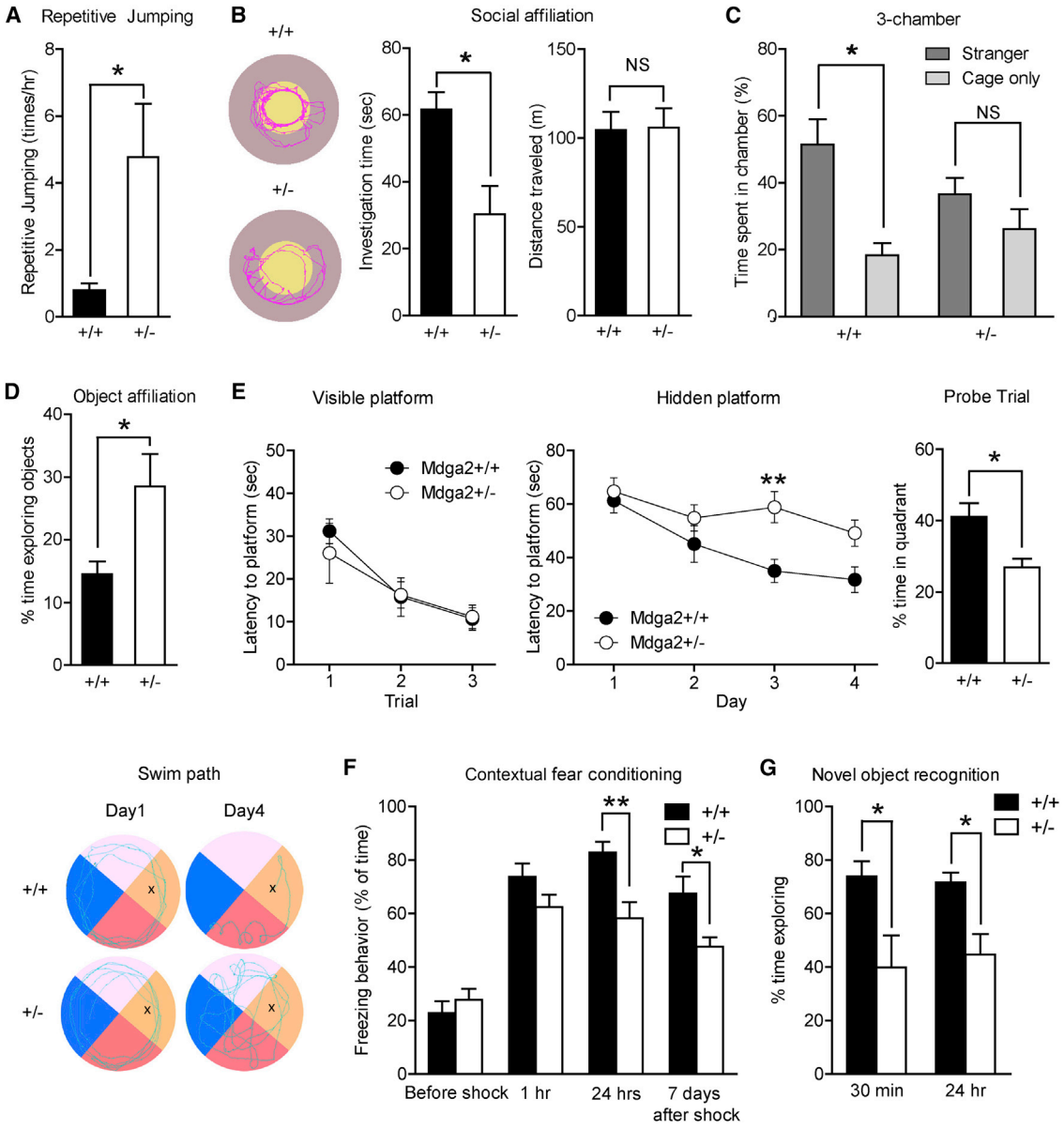

Figure 6. *Mdga2*$^{+/-}$ Mice Exhibit Motor Stereotypy and Deficits in Social Interaction and Hippocampus-Dependent Learning and Memory

(A) *Mdga2*$^{+/-}$ mice exhibited more spontaneous repetitive jumping in the home cage (unpaired t test, $t_{16} = 2.738$, *p = 0.025; n = 9 *Mdga2*$^{+/-}$ and 9 WT mice).

(B) In the representative images of paths (red) of mice examined in the social affiliation test, the pale yellow circle represents the area containing the unfamiliar mouse plus 3 cm of surround, and the brown region the remaining test field. The WT littermate investigated the unfamiliar mouse; however, the *Mdga2*$^{+/-}$ mouse kept a distance and only occasionally interacted with the unfamiliar mouse. Time spent investigating the unfamiliar mouse differed between genotypes (unpaired t test, $t_{13} = 0.992$, *p = 0.0097), but distance traveled did not differ ($t_{13} = 0.376$, p = 0.88; n = 7 *Mdga2*$^{+/-}$ and 8 WT mice).

(C) In the three-chamber test, WT mice spent more time in the chamber with the unfamiliar mouse than with the cage alone (paired t test, $t_{30} = 3.93$, *p = 0.00046), whereas *Mdga2*$^{+/-}$ mice showed little preference ($t_{32} = 1.297$, p = 0.204; n = 17 *Mdga2*$^{+/-}$ and 16 WT mice).

(D) In the object affiliation test, *Mdga2*$^{+/-}$ mice spent more time exploring non-living objects than WT littermates (unpaired t test, $t_{13} = 2.650$, *p = 0.020; n = 7 *Mdga2*$^{+/-}$ and 8 WT mice).

(E) In the MWM, no significant difference was observed in swimming speed of *Mdga2*$^{+/-}$ and WT mice (data not shown; unpaired t test, $t_{17} = 0.483$, p = 0.72; n = 7 WT and 12 *Mdga2*$^{+/-}$ mice), suggesting motor function was intact. *Mdga2*$^{+/-}$ and WT mice also showed equal performance and training in terms of latency to find a visible platform (two-way repeated-measures ANOVA, genotype $F_{1,21} = 0.21$, p = 0.65). However, *Mdga2*$^{+/-}$ mice required significantly more time to reach a hidden platform even after consecutive trials (two-way repeated-measures ANOVA, genotype $F_{1,21} = 6.493$, p = 0.019; **p < 0.01 by Bonferroni's post hoc test). In the probe trial performed 1 hr after the last trial, unlike WT mice, *Mdga2*$^{+/-}$ mice did not show a preference to stay in the target quadrant (unpaired t test, $t_{17} = 2.332$, *p = 0.032). Representative swim paths show a more directed movement of the WT mouse to the hidden platform (x).

(F) In the contextual fear conditioning task, at 24 hr and 7 days after training *Mdga2*$^{+/-}$ mice showed a significant reduction in time exhibiting freezing behavior when placed back in the test chamber (two-way ANOVA, genotype $F_{(1,104)} = 13.10$, p = 0.0005; *p < 0.05, **p < 0.01 by Bonferroni's post hoc test; n = 15 *Mdga2*$^{+/-}$

(legend continued on next page)

and to facilitate comparison with fMRI ASD studies, we employed in vivo wide-field, mesoscale, voltage-sensitive dye (VSD) imaging (Chan et al., 2015; Mohajerani et al., 2013). As previously, we used a giant, unilateral cranial window preparation that allowed us to image voltage activity of nearly the entire dorsal neocortex of the right hemisphere (Figure 7A). Both *Mdga2*$^{+/-}$ and WT mice exhibited dynamic, spatially complex patterns of spontaneous cortical activity (Figures 7B and S7). Baseline excitability was examined by computing the SD of the time course of spontaneous fluorescent voltage activity ($\Delta F/F_0$) for each pixel imaged to construct an activity map whereby the cortical regional distribution of excitability is localized. Evident from these maps is a heightened level of activity along midline regions in both genotypes but strikingly more activity in the *Mdga2*$^{+/-}$ mice (Figure 7C). To quantify these differences and to assess region-specific differences, we derived the mean SD measures of spontaneous activity from 18 regions of interest (ROIs, 0.112 mm^2) across the cortex in *Mdga2*$^{+/-}$ and WT mice (Figure 7C). ROI locations were determined by a combination of direct, multiple modality, sensory-stimulation, and extrapolated coordinates from atlases. *Mdga2*$^{+/-}$ mice exhibited significantly higher levels of baseline activity than WT mice, with significant regional increases found in pM2, RS, mBC, and mFL (Figure 7D). Nonsignificant trends toward enhanced activity were also observed in aM2/AC and mHL regions. Taken together, these data are consistent with a region-specific increase in spontaneous cortical activity due to *Mdga2* haploinsufficiency.

Imaging studies in ASD have revealed changes in resting-state activity but have focused more on functional connectivity (Hahamy et al., 2015; Uddin et al., 2013). Thus, we analyzed the effect of *Mdga2* haploinsufficiency on intrahemispheric functional connectivity through the construction of connectivity matrices derived from the cross-correlation of spontaneous activity from our previously established ROIs. Subtraction from the mean connectivity matrix generated from *Mdga2*$^{+/-}$ mice (Figure 8A) by the mean connectivity matrix from WT mice (Figure 8B) yielded a difference connectivity matrix that revealed a global increase in mean functional connectivity in *Mdga2*$^{+/-}$ ($MeanCorr_{Mdga2^{+/-}}$ = 0.6666 ± 0.0034 versus $MeanCorr_{wild\text{-}type}$ = 0.6028 ± 0.0038, n_{corr} = 1,530; Figure 8C). Functional connectivity strength was most strongly enhanced in *Mdga2*$^{+/-}$ lateral cortical areas encompassing secondary somatosensory cortices (HLS2A, HLS2B, FLS2, and BCS2) and primary auditory cortex, relative to WT ($LateralMeanCorr_{Mdga2^{+/-}}$ = 0.6770 ± 0.0050 versus $LateralMeanCorr_{wild\text{-}type}$ = 0.5959 ± 0.0053, n_{corr} = 680). Results of the cross-correlation comparison are represented in a network diagram of functional connectivity (Figure 8D) whereby node sizes are proportional to the number of connections and node position by the location the cortical region represented. Connections between nodes demonstrating enhanced functional connectivity (>15%) in *Mdga2*$^{+/-}$ cortex relative to WT are delineated by green. Changes in functional connectivity of less than 15% are shown with gray lines. No losses in functional connectivity strength exceeding 15% were observed. These data suggest that MDGA2 plays a role in downregulating functional connectivity between cortical nodes related to sensory processing.

DISCUSSION

Mdga2$^{+/-}$ mice described here may serve as a useful model for ASD, mimicking single-allele truncating mutations (Bucan et al., 2009), and exhibiting stereotypy, social interaction deficits, and altered cognition. Validity may be further supported by the functional imaging: the increased SD of recorded spontaneous activity and functional hyperconnectivity in *Mdga2*$^{+/-}$ cortex parallel the increased amplitude of low-frequency fluctuations (ALFFs) and hyperconnectivity observed in some fMRI studies of ASD (Supekar et al., 2013). Mechanistically, we show that (1) MDGA2 complexes with NL1 and NL2, inhibits their interaction with Nrx, and inhibits their synaptogenic activity; (2) MDGA2 overexpression suppresses synapse development; (3) *Mdga2*$^{+/-}$ hippocampal CA1 neurons exhibit elevated excitatory synapse density, mEPSC frequency and amplitude, input/output response, surface synaptic GluA1, AMPA/NMDA ratio, and E-LTP but defective L-LTP; and (4) resting-state activity is elevated in multiple cortical regions of *Mdga2*$^{+/-}$ mice, and intrahemispheric functional connectivity is increased. Consistent with these findings in *Mdga2*$^{+/-}$ mice, in addition to deletions in ASD a de novo deletion in *MDGA2* was found in epileptic encephalopathy (Lesca et al., 2012). Thus, *MDGA2* functions in the *NRXN-NLGN-SHANK* pathway but in an unusual capacity, as a suppressor of excitatory synapse development. Paradoxically, whereas ASD-associated mutations in *NRXN*s and *SHANK*s diminish function of this pathway to reduce E/I ratio (Etherton et al., 2009; Glessner et al., 2009; Jiang and Ehlers, 2013), ASD-associated mutations in *MDGA2* enhance function of this pathway to elevate E/I ratio. These findings imply that perturbations of this synaptic pathway in either direction from the norm increase risk for ASD.

Although many proteins are known to promote excitatory synapse development, information about suppressors has been lacking in mammalian systems. Other proteins that limit excitatory synapse density work through indirect mechanisms and affect other processes such as neuron arbor development. For example, transcription factor MEF2 acts through FMRP, mGluR5, and Arc (Wilkerson et al., 2014), and Ephexin5 and Nogo receptors both act through RhoA GTPase (Margolis et al., 2010; Wills et al., 2012). MDGAs appear to play a specific role in suppressing synapse development by blocking binding of Nrx to NLs on the plasma membrane. If the localization observed for recombinant MDGA2 is representative of the native distribution, MDGA2 may interact with extrasynaptic

and 13 WT mice). There was no difference in freezing response to the initial shock, assessed either as duration of first freeze or as percent time frozen in the 30 s following the shock (both $p > 0.5$; data not shown).

(G) In the novel object recognition test, of the time exploring objects, WT mice spent a greater fraction of time exploring the novel object at both 30 min and 24 hr after the last training session. However, *Mdga2*$^{+/-}$ mice did not show a preference for the novel object over a familiar object (two-way ANOVA, genotype $F_{1,26}$ = 14.63, $p = 0.0007$; *$p < 0.05$ by Bonferroni's post hoc test; n = 7 *Mdga2*$^{+/-}$ and 8 WT mice).

Error bars indicate SEM. See also Figures S5 and S6.

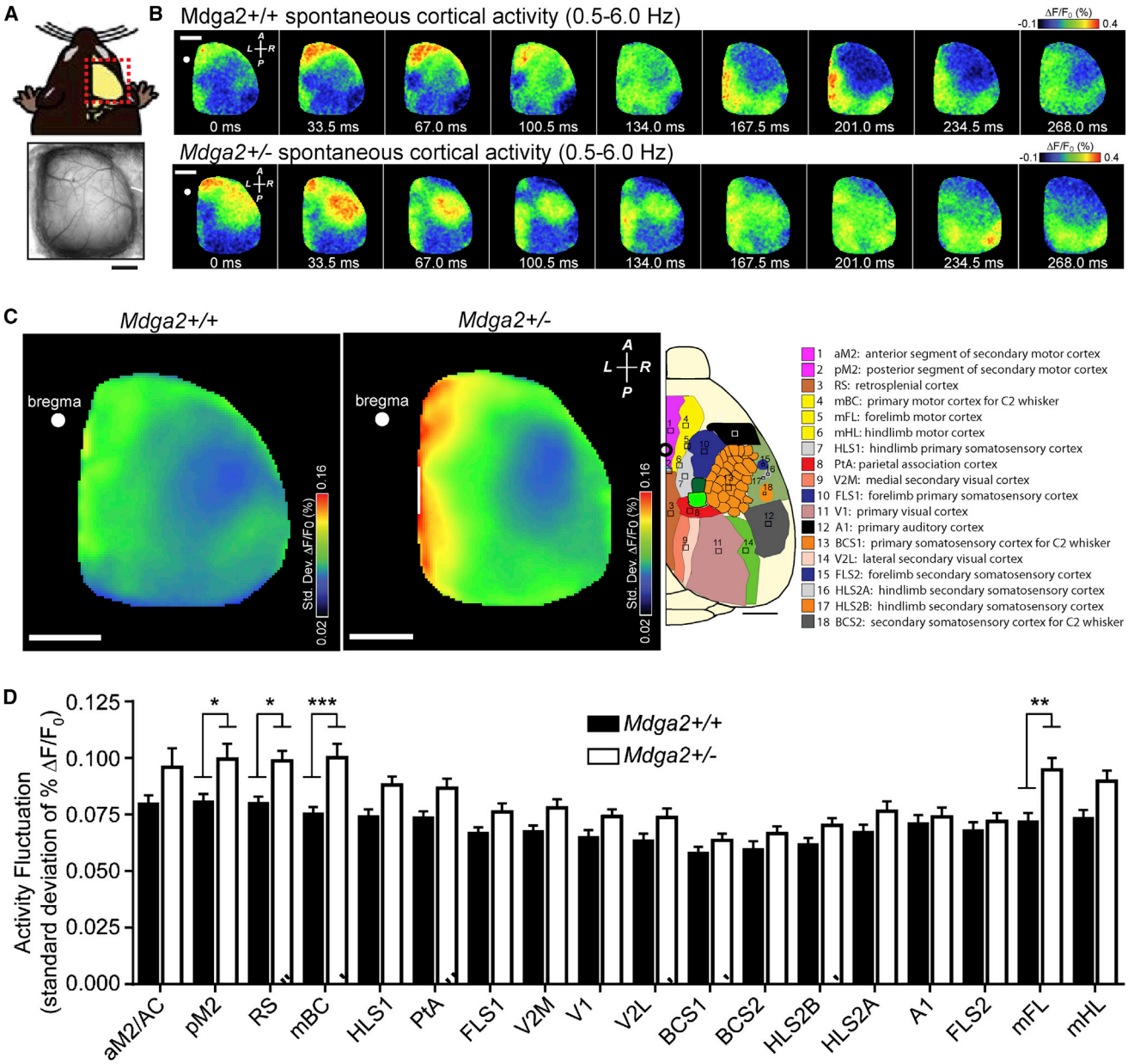

Figure 7. Wide-Field VSD Imaging of Spontaneous Activity Reveals Enhanced Regional Resting-State Activity in *Mdga2*$^{+/-}$ Mouse Cortex

(A) Top: cartoon illustrating the perspective and field of view (dashed red box) used to image voltage activity. Bottom: exemplar image of the cortical surface as viewed through the cranial window (scale bar, 2 mm).

(B) Montage over time of VSD imaging of a segment of spontaneous cortical activity from *Mdga2*$^{+/-}$ and WT mice illustrating dynamic and spatially complex activity. Amplitude of fluorescent voltage signal (%ΔF/F0) scaled to color bar.

(C) Exemplar map of spontaneous activity illustrating regional differences derived from the SD of recorded spontaneous activity for *Mdga2*$^{+/-}$ and WT mice (scale bar, 2 mm). White circle denotes position of the bregma. Compass points indicate anterior (A), posterior (P), left (L), and right (R) directions. Right: schematic of cortical imaging field of view illustrating positions of regions of interest (ROIs).

(D) Mean activity derived from 18 ROIs (0.112 mm^2) described in (C) indicated increased activity in medial cortical regions including pM2, RS, mBC, and mFL in *Mdga2*$^{+/-}$ (n = 10) relative to WT (n = 10) mice (two-way ANOVA, genotype $p < 0.0001$; *$p < 0.05$, **$p < 0.01$, ***$p < 0.001$, with Bonferroni's post hoc test). Error bars indicate SEM. See also Figure S7.

NL1, facilitated by the high mobility of surface NL1 (Chamma et al., 2016).

In *Mdga2*$^{+/-}$ mice we observed a selective enhancement of excitatory, but not inhibitory, synapses. Yet MDGA2 suppressed the synaptogenic activity of both NL1 and NL2 in co-culture, and MDGA2 overexpression suppressed excitatory and inhibitory synapse development. We suggest that MDGA1 may be sufficient to maintain normal inhibitory synapse density

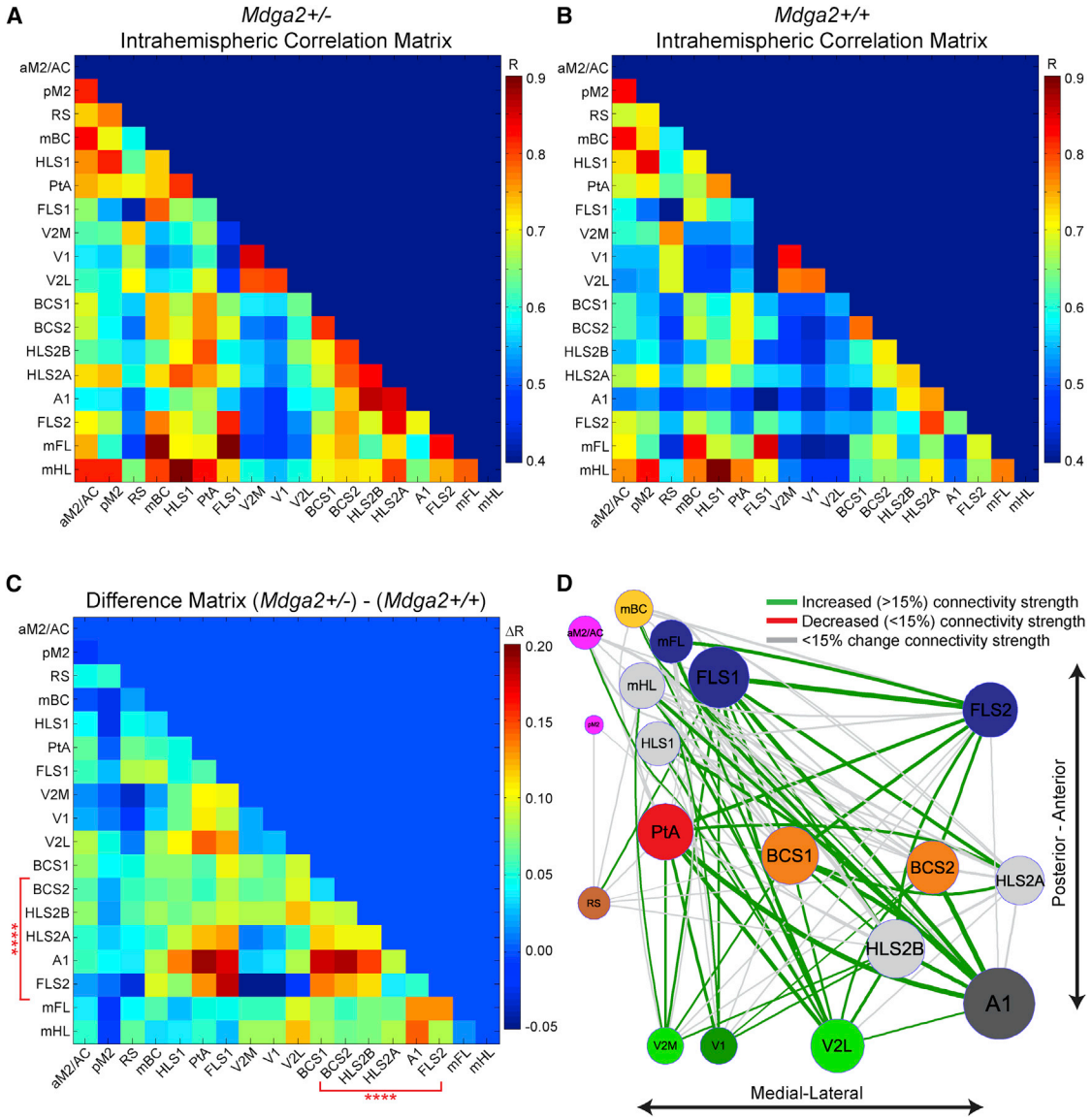

Figure 8. *Mdga2*$^{+/-}$ Mice Exhibit Enhanced Intrahemispheric Functional Connectivity

(A–C) Intrahemispheric functional connectivity matrices were derived from the cross-correlation of 18 ROIs (described in Figure 6C) from VSD imaging of spontaneous activity from anesthetized *Mdga2*$^{+/-}$ (n = 10) and WT mice (n = 10). The difference correlation matrix (C), obtained by subtracting the mean WT from the mean *Mdga2*$^{+/-}$ correlation matrix, reveals a global increase in mean functional connectivity ($MeanCorr_{MDGA2}{}^{+/-} = 0.6666 \pm 0.0034$ versus $MeanCorr_{wild\text{-}type} = 0.6028 \pm 0.0038$, $n_{corr} = 1{,}530$; $p < 0.0001$, Wilcoxon rank-sum test). Lateral cortical ROIs, denoted by red brackets, including secondary somatosensory cortices (HLS2A, HLS2B, FLS2, and BCS2) and primary auditory cortex (A1), exhibited enhanced functional connectivity strength in the *Mdga2*$^{+/-}$ population compared to WT ($LateralMeanCorr_{MDGA2}{}^{+/-} = 0.6770 \pm 0.0050$ versus $LateralMeanCorr_{wild\text{-}type} = 0.5959 \pm 0.0053$, $n_{corr} = 680$; $p < 0.0001$, Wilcoxon rank-sum test). Correlation coefficients (A and B) or their difference (C) are represented by color (R or ΔR bars). Self-correlated ROIs forming the diagonal have been omitted.

(D) Network diagram of functional connectivity derived from the difference correlation matrix in (C). Node locations reflect spatial organization according to experimentally derived locations and atlas coordinates with size proportional to the strength of connections per node. Green lines indicate enhanced functional connectivity (>15%) between nodes in *Mdga2*$^{+/-}$ mice with respect to WT; reductions >15% were not observed. Gray lines indicate changes in functional connectivity of less than 15%.

upon genetic reduction of MDGA2. MDGA1 also suppresses the synaptogenic activity of NL2 in co-culture (Pettem et al., 2013b) (and Figure 1), and MDGA1 is highly expressed by hippocampal CA1 pyramidal neurons and broadly in cortex (Ishikawa et al., 2011; Litwack et al., 2004). Moreover, knockdown of MDGA1 in *Mdga2*$^{+/-}$ neurons increased functional inhibitory synapses with no effect on excitatory synapses (Figure 4). However, further studies are needed to determine whether MDGA2 may play a subtle masked role or no role at inhibitory synapses, and more generally to better understand the structural, cellular, and circuit basis of selective roles of MDGA family proteins.

Consistent with the function of MDGA2 to suppress NL1-Nrx interaction, *Mdga2*$^{+/-}$ mice share some phenotypes with transgenic mice overexpressing NL1, namely an increase in excitatory synapse density, increased input/output response, and learning deficits in the MWM (Dahlhaus et al., 2010). NL1 overexpression can increase AMPA/NMDA ratio (Schnell et al., 2012), and NL1 recruits AMPA receptors through PSD-95 family MAGUKs (Mondin et al., 2011). The increased levels of PSD-95 family MAGUKs observed here may contribute to the increase in surface synaptic GluA1, mEPSC amplitude, and AMPA/NMDA ratio observed in *Mdga2*$^{+/-}$ neurons. We observed little effect of *Mdga2* haploinsufficiency on presynaptic release properties, similar to NL1 overexpression in vivo (Dahlhaus et al., 2010; Schnell et al., 2012). Interestingly, whereas NL1 transgenic mice showed a simple deficit in LTP, the effect of *Mdga2* haploinsufficiency on synaptic plasticity was more complex.

Mdga2$^{+/-}$ mice exhibited enhanced potentiation in an E-LTP paradigm but a significant reduction in the maintenance of potentiation in an L-LTP paradigm. These two forms of LTP involve different mechanisms. Generally, E-LTP is mediated by changes in AMPA receptor trafficking whereas L-LTP requires protein synthesis (Reymann and Frey, 2007; Takeuchi et al., 2013). In *Mdga2*$^{+/-}$ mice, the increased basal excitation and synapse density may contribute to cooperativity during stimulation, resulting in more robust E-LTP, but signaling mechanisms required for L-LTP may be compromised. Supporting this idea, other models that exhibit normal or enhanced E-LTP together with deficient L-LTP include mice expressing an inhibitory regulatory subunit of PKA or lacking GCN2 kinase or Rictor mTORC2 component (Abel et al., 1997; Costa-Mattioli et al., 2005; Huang et al., 2013). All of these mouse models exhibited memory deficits, supporting the widely held notion that L-LTP may underlie memory (Takeuchi et al., 2013). The cognitive deficits in *Mdga2*$^{+/-}$ mice observed in the MWM, contextual fear conditioning, and novel object recognition may likewise reflect the deficit in L-LTP or underlying alterations in shared molecular signaling pathways. Alternatively, the deficit in novel object recognition might be more related to restricted interests as suggested for another mouse model relevant to ASD (Kane et al., 2012).

The *Mdga2*$^{+/-}$ mouse model, with elevated E/I ratio, represents a distinct contrast to most other models of ASD in the *NRXN-NLGN-DLG-DLGAP-SHANK* synaptic pathway, which exhibit reduced E/I ratios. Two other interesting exceptions are *Nlgn4*$^{-/-}$ and *Syngap1*$^{+/-}$ mice. *Nlgn4*$^{-/-}$ mice show a mild impairment in inhibitory transmission associated with a severe impairment in γ-oscillations (Hammer et al., 2015) and may be mechanistically similar to models with reduced numbers of interneurons. Like *Mdga2*, complete knockout of *Syngap1* is lethal, and haploinsufficiency results in behavioral deficits (Komiyama et al., 2002; Ogden et al., 2016). However, *Syngap1*$^{+/-}$ mice exhibit elevated E/I ratio only transiently during development and SYNGAP regulates GTPase signaling, perhaps contributing to the association of *SYNGAP1* mutations with a broader disease spectrum (Ogden et al., 2016).

The application of meso- and macroscopic functional imaging to intact mouse models of ASD has been limited. Conventional neuroimaging approaches such as fMRI most frequently used in human populations have limited temporal resolution and have more limited efficacy in small animal models where spatial resolution is often insufficient to resolve regional-scale activity. However, the advent of ultra-high-field fMRI is facilitating such studies and has revealed increased local functional connectivity in sensory cortices in acallosal BTBR mice (Dodero et al., 2013). More spatially targeted imaging has described consistent features of enhanced connectivity in sensory cortex in fragile X models (Gonçalves et al., 2013; Zhang et al., 2014). Intrinsic signal imaging in BTBR mice also revealed deficits in multisensory integration in insular cortex that resulted from impaired inhibitory drive (Gogolla et al., 2014). These targeted functional imaging studies using ASD mouse models re-affirm consistent features of cortical hyper-excitability and elevated functional connectivity. The application of wide-field VSD imaging as performed here can provide a basis for broadly assessing cortical excitability and functional connectivity with high spatiotemporal resolution.

Two striking findings arose from our VSD imaging of *Mdga2*$^{+/-}$ mice: enhanced resting-state cortical activity and functional intrahemispheric hyperconnectivity. The midline regions exhibiting enhanced activity are associated with a proposed rodent analog of the default mode network, a network that exhibits low activity during goal-directed tasks and is thought to function in reflection and conceptual processing (Lu et al., 2012). Consistent with the enhanced cortical activity observed here, a recent analysis of task-free resting-state fMRI (rs-fMRI) data revealed an increase in global mean ALFF, indicating enhanced activity in children with ASD compared with typically developing children (Supekar et al., 2013). A large-scale rs-fMRI study associated with the Autism Brain Imaging Data Exchange (ABIDE) also reported a large middle frontal region of enhanced ALFF, and a smaller occipital region of reduced ALFF, associated with ASD (Di Martino et al., 2014).

Most fMRI studies in ASD have focused on functional connectivity, with variable findings. Reports of hypo-connectivity have tended to predominate (Uddin et al., 2013). However, more in keeping with our findings in the *Mdga2*$^{+/-}$ model, two recent studies of children with ASD reported an overall increase in functional connectivity, and in both studies the degree of hyperconnectivity correlated with symptom severity (Keown et al., 2013; Supekar et al., 2013). Perhaps the largest study, using the ABIDE database, found neither hypo- nor hyperconnectivity on a global scale, but rather idiosyncratic distortions, i.e., greater variations from the mean in individuals of the ASD group (Hahamy et al., 2015).

An important consideration in the interpretation of our connectivity analyses in the context of rs-fMRI studies is that we imaged membrane potential changes as opposed to blood-oxygenation-level-dependent (BOLD) contrast imaging used in fMRI. While the underlying neural activity correlate of spontaneous BOLD signals is unclear, electrophysiological correlates such as slow cortical potentials and infraslow EEG fluctuations, among others, have been identified (He et al., 2008; Hiltunen et al., 2014; Logothetis, 2008). We recently demonstrated that the functional organization of infraslow spontaneous VSD activity resembled the higher-frequency activity described here and previously, providing us with confidence that these large resting-state network structures are preserved and observable

across imaging modalities (Chan et al., 2015; Mohajerani et al., 2013). The diversity of ASD findings with respect to connectivity observed using rs-fMRI may reflect the heterogeneity of disease mechanisms and emphasizes the need to correlate imaging, complemented by diverse neuronal activity reporters such as VSD, with behavior, biomarkers, and genetics.

In conclusion, our results demonstrate a novel mechanism through which the genetic pathway mediating E/I balance can be disrupted and how this alteration contributes to ASD phenotypes ranging from the molecular to the systems level. Although the majority of data investigating NLs suggests that mutations or changes in absolute levels of NLs or their effectors contribute to autism, our data represent an alternative but complementary model in which disinhibition of NL function through loss of endogenous regulators may yield autism phenotypes. The approach presented here for assessing wide-field regional cortical activity and functional connectivity with high spatiotemporal resolution may also prove useful in assessing other mouse models of neuropsychiatric disorders. Such parallel animal imaging studies in genetically based ASD models may reciprocally guide approaches in human imaging studies to better understand disease etiology, identify biomarkers, and eventually develop individualized treatments.

EXPERIMENTAL PROCEDURES

Experimental procedures are described in detail in the Supplemental Experimental Procedures. All values are presented as mean ± SEM.

Cell culture, immunofluorescence, co-immunoprecipitation, and binding assays were performed essentially as described (Linhoff et al., 2009; Pettem et al., 2013b; Siddiqui et al., 2013). Imaging and analysis were performed blind to transfection group.

Animal care and use protocols were approved by the respective host institutions. MDGA2 null mice were generated and backcrossed to C57BL/6 for at least ten generations. Assays were performed on adult mice (6–10 weeks old) unless otherwise indicated. In situ hybridization, β-galactosidase activity staining, western blotting, electron microscopy, and electrophysiology followed previous methods (Ishikawa et al., 2011; Pettem et al., 2013a; Siddiqui et al., 2013).

All behavioral studies were performed blind to genotype, following previous protocols (Kishimoto et al., 2015) and Supplemental Information.

In vivo VSD imaging of anesthetized mice was performed essentially as previously described (Chan et al., 2015; Mohajerani et al., 2013). VSD was applied to the exposed cortex, staining all neocortical layers and images captured at 150 Hz with a CCD focused into the cortex to a depth of ~1 mm. VSD responses were expressed as a percent change relative to baseline, $(F - F_0)/F_0*100$. Network analysis was performed using custom MATLAB scripts (Lim et al., 2015; http://www.neuroscience.ubc.ca/faculty/murphy_software.html) and the Brain Connectivity Toolbox.

SUPPLEMENTAL INFORMATION

Supplemental Information includes Supplemental Experimental Procedures and seven figures and can be found with this article online at http://dx.doi.org/10.1016/j.neuron.2016.08.016.

AUTHOR CONTRIBUTIONS

S.A.C., I.A.-J., T.Y., and A.M.C. conceived the project. Experiments were designed, performed, and analyzed by I.A.-J., Y.G., and A.M.C. (Figure 1); H.L., S.A.C., Y.G., and A.M.C. (Figure 2); I.A.-J., S.A.C., R.Y., A.M.C., C.M., H.M., H.K., F.M., T.S., and T.Y. (Figure 3); S.A.C., Y.G., A.M.C., and Y.T.W. (Figure 4); S.A.C., H.L., Y.G., A.M.C., and Y.T.W. (Figure 5); Y. Kishimoto, C.M., N.K., A.T., Y. Kirino, and T.Y. (Figure 6); and A.W.C., J.M.L., and T.H.M. (Figures 7 and 8). S.A.C. and A.M.C. wrote the manuscript with contributions from A.W.C. and T.Y. and input from all authors.

ACKNOWLEDGMENTS

We thank Xiling Zhou, Nazarine Fernandes, Pumin Wang, Ayumi Hamada, Tadahiro Nakajima, and Daiki Ojima for excellent technical assistance. This work was supported by a Brain Canada and Genome BC MIRI Award (A.M.C. and T.H.M.), Canadian Institutes of Health Research MOP 125965 and FDN 143206 and a Canada Research Chair Award (A.M.C.), Grants-in-Aid for Scientific Research 15K07910 (Y. Kishimoto) and 25460059 (T.Y.) from Japan Society for the Promotion of Science, a Brain Canada Bell Mental Health Fellowship (S.A.C.), and a Lundbeck Foundation Fellowship (I.A.-J.).

Received: February 26, 2016
Revised: June 13, 2016
Accepted: July 29, 2016
Published: September 7, 2016

REFERENCES

Abel, T., Nguyen, P.V., Barad, M., Deuel, T.A., Kandel, E.R., and Bourtchouladze, R. (1997). Genetic demonstration of a role for PKA in the late phase of LTP and in hippocampus-based long-term memory. Cell *88*, 615–626.

American Psychiatric Association (2000). Diagnostic and Statistical Manual of Mental Disorders, Fourth Edition (American Psychiatric Publishing).

Amiet, C., Gourfinkel-An, I., Bouzamondo, A., Tordjman, S., Baulac, M., Lechat, P., Mottron, L., and Cohen, D. (2008). Epilepsy in autism is associated with intellectual disability and gender: evidence from a meta-analysis. Biol. Psychiatry *64*, 577–582.

Béna, F., Bruno, D.L., Eriksson, M., van Ravenswaaij-Arts, C., Stark, Z., Dijkhuizen, T., Gerkes, E., Gimelli, S., Ganesamoorthy, D., Thuresson, A.C., et al. (2013). Molecular and clinical characterization of 25 individuals with exonic deletions of NRXN1 and comprehensive review of the literature. Am. J. Med. Genet. B. Neuropsychiatr. Genet. *162B*, 388–403.

Blundell, J., Blaiss, C.A., Etherton, M.R., Espinosa, F., Tabuchi, K., Walz, C., Bolliger, M.F., Südhof, T.C., and Powell, C.M. (2010). Neuroligin-1 deletion results in impaired spatial memory and increased repetitive behavior. J. Neurosci. *30*, 2115–2129.

Bourgeron, T. (2015). From the genetic architecture to synaptic plasticity in autism spectrum disorder. Nat. Rev. Neurosci. *16*, 551–563.

Bucan, M., Abrahams, B.S., Wang, K., Glessner, J.T., Herman, E.I., Sonnenblick, L.I., Alvarez Retuerto, A.I., Imielinski, M., Hadley, D., Bradfield, J.P., et al. (2009). Genome-wide analyses of exonic copy number variants in a family-based study point to novel autism susceptibility genes. PLoS Genet. *5*, e1000536.

Chamma, I., Letellier, M., Butler, C., Tessier, B., Lim, K.H., Gauthereau, I., Choquet, D., Sibarita, J.B., Park, S., Sainlos, M., and Thoumine, O. (2016). Mapping the dynamics and nanoscale organization of synaptic adhesion proteins using monomeric streptavidin. Nat. Commun. *7*, 10773.

Chan, A.W., Mohajerani, M.H., LeDue, J.M., Wang, Y.T., and Murphy, T.H. (2015). Mesoscale infraslow spontaneous membrane potential fluctuations recapitulate high-frequency activity cortical motifs. Nat. Commun. *6*, 7738.

Chen, J.A., Peñagarikano, O., Belgard, T.G., Swarup, V., and Geschwind, D.H. (2015). The emerging picture of autism spectrum disorder: genetics and pathology. Annu. Rev. Pathol. *10*, 111–144.

Cohen, S.J., and Stackman, R.W., Jr. (2015). Assessing rodent hippocampal involvement in the novel object recognition task. A review. Behav. Brain Res. *285*, 105–117.

Costa-Mattioli, M., Gobert, D., Harding, H., Herdy, B., Azzi, M., Bruno, M., Bidinosti, M., Ben Mamou, C., Marcinkiewicz, E., Yoshida, M., et al. (2005).

Translational control of hippocampal synaptic plasticity and memory by the eIF2alpha kinase GCN2. Nature *436*, 1166–1173.

Dahlhaus, R., Hines, R.M., Eadie, B.D., Kannangara, T.S., Hines, D.J., Brown, C.E., Christie, B.R., and El-Husseini, A. (2010). Overexpression of the cell adhesion protein neuroligin-1 induces learning deficits and impairs synaptic plasticity by altering the ratio of excitation to inhibition in the hippocampus. Hippocampus *20*, 305–322.

Di Martino, A., Yan, C.G., Li, Q., Denio, E., Castellanos, F.X., Alaerts, K., Anderson, J.S., Assaf, M., Bookheimer, S.Y., Dapretto, M., et al. (2014). The autism brain imaging data exchange: towards a large-scale evaluation of the intrinsic brain architecture in autism. Mol. Psychiatry *19*, 659–667.

Dodero, L., Damiano, M., Galbusera, A., Bifone, A., Tsaftsaris, S.A., Scattoni, M.L., and Gozzi, A. (2013). Neuroimaging evidence of major morpho-anatomical and functional abnormalities in the BTBR T+TF/J mouse model of autism. PLoS ONE *8*, e76655.

Etherton, M.R., Blaiss, C.A., Powell, C.M., and Südhof, T.C. (2009). Mouse neurexin-1alpha deletion causes correlated electrophysiological and behavioral changes consistent with cognitive impairments. Proc. Natl. Acad. Sci. USA *106*, 17998–18003.

Giannone, G., Mondin, M., Grillo-Bosch, D., Tessier, B., Saint-Michel, E., Czöndör, K., Sainlos, M., Choquet, D., and Thoumine, O. (2013). Neurexin-1β binding to neuroligin-1 triggers the preferential recruitment of PSD-95 versus gephyrin through tyrosine phosphorylation of neuroligin-1. Cell Rep. *3*, 1996–2007.

Glessner, J.T., Wang, K., Cai, G., Korvatska, O., Kim, C.E., Wood, S., Zhang, H., Estes, A., Brune, C.W., Bradfield, J.P., et al. (2009). Autism genome-wide copy number variation reveals ubiquitin and neuronal genes. Nature *459*, 569–573.

Gogolla, N., Takesian, A.E., Feng, G., Fagiolini, M., and Hensch, T.K. (2014). Sensory integration in mouse insular cortex reflects GABA circuit maturation. Neuron *83*, 894–905.

Gonçalves, J.T., Anstey, J.E., Golshani, P., and Portera-Cailliau, C. (2013). Circuit level defects in the developing neocortex of fragile X mice. Nat. Neurosci. *16*, 903–909.

Hahamy, A., Behrmann, M., and Malach, R. (2015). The idiosyncratic brain: distortion of spontaneous connectivity patterns in autism spectrum disorder. Nat. Neurosci. *18*, 302–309.

Hammer, M., Krueger-Burg, D., Tuffy, L.P., Cooper, B.H., Taschenberger, H., Goswami, S.P., Ehrenreich, H., Jonas, P., Varoqueaux, F., Rhee, J.S., and Brose, N. (2015). Perturbed hippocampal synaptic inhibition and γ-oscillations in a neuroligin-4 knockout mouse model of autism. Cell Rep. *13*, 516–523.

He, B.J., Snyder, A.Z., Zempel, J.M., Smyth, M.D., and Raichle, M.E. (2008). Electrophysiological correlates of the brain's intrinsic large-scale functional architecture. Proc. Natl. Acad. Sci. USA *105*, 16039–16044.

Hiltunen, T., Kantola, J., Abou Elseoud, A., Lepola, P., Suominen, K., Starck, T., Nikkinen, J., Remes, J., Tervonen, O., Palva, S., et al. (2014). Infra-slow EEG fluctuations are correlated with resting-state network dynamics in fMRI. J. Neurosci. *34*, 356–362.

Huang, Y.Y., and Kandel, E.R. (1994). Recruitment of long-lasting and protein kinase A-dependent long-term potentiation in the CA1 region of hippocampus requires repeated tetanization. Learn. Mem. *1*, 74–82.

Huang, W., Zhu, P.J., Zhang, S., Zhou, H., Stoica, L., Galiano, M., Krnjević, K., Roman, G., and Costa-Mattioli, M. (2013). mTORC2 controls actin polymerization required for consolidation of long-term memory. Nat. Neurosci. *16*, 441–448.

Irie, M., Hata, Y., Takeuchi, M., Ichtchenko, K., Toyoda, A., Hirao, K., Takai, Y., Rosahl, T.W., and Südhof, T.C. (1997). Binding of neuroligins to PSD-95. Science *277*, 1511–1515.

Ishikawa, T., Gotoh, N., Murayama, C., Abe, T., Iwashita, M., Matsuzaki, F., Suzuki, T., and Yamamoto, T. (2011). IgSF molecule MDGA1 is involved in radial migration and positioning of a subset of cortical upper-layer neurons. Dev. Dyn. *240*, 96–107.

Jiang, Y.H., and Ehlers, M.D. (2013). Modeling autism by SHANK gene mutations in mice. Neuron *78*, 8–27.

Kane, M.J., Angoa-Peréz, M., Briggs, D.I., Sykes, C.E., Francescutti, D.M., Rosenberg, D.R., and Kuhn, D.M. (2012). Mice genetically depleted of brain serotonin display social impairments, communication deficits and repetitive behaviors: possible relevance to autism. PLoS ONE *7*, e48975.

Keown, C.L., Shih, P., Nair, A., Peterson, N., Mulvey, M.E., and Müller, R.A. (2013). Local functional overconnectivity in posterior brain regions is associated with symptom severity in autism spectrum disorders. Cell Rep. *5*, 567–572.

Kishimoto, Y., Cagniard, B., Yamazaki, M., Nakayama, J., Sakimura, K., Kirino, Y., and Kano, M. (2015). Task-specific enhancement of hippocampus-dependent learning in mice deficient in monoacylglycerol lipase, the major hydrolyzing enzyme of the endocannabinoid 2-arachidonoylglycerol. Front. Behav. Neurosci. *9*, 134.

Komiyama, N.H., Watabe, A.M., Carlisle, H.J., Porter, K., Charlesworth, P., Monti, J., Strathdee, D.J., O'Carroll, C.M., Martin, S.J., Morris, R.G., et al. (2002). SynGAP regulates ERK/MAPK signaling, synaptic plasticity, and learning in the complex with postsynaptic density 95 and NMDA receptor. J. Neurosci. *22*, 9721–9732.

Krueger, D.D., Tuffy, L.P., Papadopoulos, T., and Brose, N. (2012). The role of neurexins and neuroligins in the formation, maturation, and function of vertebrate synapses. Curr. Opin. Neurobiol. *22*, 412–422.

Leblond, C.S., Nava, C., Polge, A., Gauthier, J., Huguet, G., Lumbroso, S., Giuliano, F., Stordeur, C., Depienne, C., Mouzat, K., et al. (2014). Meta-analysis of SHANK mutations in autism spectrum disorders: a gradient of severity in cognitive impairments. PLoS Genet. *10*, e1004580.

Lee, I., and Kesner, R.P. (2004). Differential contributions of dorsal hippocampal subregions to memory acquisition and retrieval in contextual fear-conditioning. Hippocampus *14*, 301–310.

Lee, K., Kim, Y., Lee, S.J., Qiang, Y., Lee, D., Lee, H.W., Kim, H., Je, H.S., Südhof, T.C., and Ko, J. (2013). MDGAs interact selectively with neuroligin-2 but not other neuroligins to regulate inhibitory synapse development. Proc. Natl. Acad. Sci. USA *110*, 336–341.

Lesca, G., Rudolf, G., Labalme, A., Hirsch, E., Arzimanoglou, A., Genton, P., Motte, J., de Saint Martin, A., Valenti, M.P., Boulay, C., et al. (2012). Epileptic encephalopathies of the Landau-Kleffner and continuous spike and waves during slow-wave sleep types: genomic dissection makes the link with autism. Epilepsia *53*, 1526–1538.

Lim, D.H., LeDue, J.M., and Murphy, T.H. (2015). Network analysis of mesoscale optical recordings to assess regional, functional connectivity. Neurophotonics *2*, 041405.

Linhoff, M.W., Laurén, J., Cassidy, R.M., Dobie, F.A., Takahashi, H., Nygaard, H.B., Airaksinen, M.S., Strittmatter, S.M., and Craig, A.M. (2009). An unbiased expression screen for synaptogenic proteins identifies the LRRTM protein family as synaptic organizers. Neuron *61*, 734–749.

Litwack, E.D., Babey, R., Buser, R., Gesemann, M., and O'Leary, D.D. (2004). Identification and characterization of two novel brain-derived immunoglobulin superfamily members with a unique structural organization. Mol. Cell. Neurosci. *25*, 263–274.

Logothetis, N.K. (2008). What we can do and what we cannot do with fMRI. Nature *453*, 869–878.

Lu, H., Zou, Q., Gu, H., Raichle, M.E., Stein, E.A., and Yang, Y. (2012). Rat brains also have a default mode network. Proc. Natl. Acad. Sci. USA *109*, 3979–3984.

Margolis, S.S., Salogiannis, J., Lipton, D.M., Mandel-Brehm, C., Wills, Z.P., Mardinly, A.R., Hu, L., Greer, P.L., Bikoff, J.B., Ho, H.Y., et al. (2010). EphB-mediated degradation of the RhoA GEF Ephexin5 relieves a developmental brake on excitatory synapse formation. Cell *143*, 442–455.

Mohajerani, M.H., Chan, A.W., Mohsenvand, M., LeDue, J., Liu, R., McVea, D.A., Boyd, J.D., Wang, Y.T., Reimers, M., and Murphy, T.H. (2013). Spontaneous cortical activity alternates between motifs defined by regional axonal projections. Nat. Neurosci. *16*, 1426–1435.

Mondin, M., Labrousse, V., Hosy, E., Heine, M., Tessier, B., Levet, F., Poujol, C., Blanchet, C., Choquet, D., and Thoumine, O. (2011). Neurexin-neuroligin adhesions capture surface-diffusing AMPA receptors through PSD-95 scaffolds. J. Neurosci. *31*, 13500–13515.

Nelson, S.B., and Valakh, V. (2015). Excitatory/inhibitory balance and circuit homeostasis in autism spectrum disorders. Neuron *87*, 684–698.

Ogden, K.K., Ozkan, E.D., and Rumbaugh, G. (2016). Prioritizing the development of mouse models for childhood brain disorders. Neuropharmacology *100*, 2–16.

Peça, J., and Feng, G. (2012). Cellular and synaptic network defects in autism. Curr. Opin. Neurobiol. *22*, 866–872.

Perez-Garcia, C.G., and O'Leary, D.D. (2016). Formation of the cortical subventricular zone requires MDGA1-mediated aggregation of basal progenitors. Cell Rep. *14*, 560–571.

Pettem, K.L., Yokomaku, D., Luo, L., Linhoff, M.W., Prasad, T., Connor, S.A., Siddiqui, T.J., Kawabe, H., Chen, F., Zhang, L., et al. (2013a). The specific α-neurexin interactor calsyntenin-3 promotes excitatory and inhibitory synapse development. Neuron *80*, 113–128.

Pettem, K.L., Yokomaku, D., Takahashi, H., Ge, Y., and Craig, A.M. (2013b). Interaction between autism-linked MDGAs and neuroligins suppresses inhibitory synapse development. J. Cell Biol. *200*, 321–336.

Reymann, K.G., and Frey, J.U. (2007). The late maintenance of hippocampal LTP: requirements, phases, 'synaptic tagging', 'late-associativity' and implications. Neuropharmacology *52*, 24–40.

Rubenstein, J.L., and Merzenich, M.M. (2003). Model of autism: increased ratio of excitation/inhibition in key neural systems. Genes Brain Behav. *2*, 255–267.

Schnell, E., Bensen, A.L., Washburn, E.K., and Westbrook, G.L. (2012). Neuroligin-1 overexpression in newborn granule cells in vivo. PLoS ONE *7*, e48045.

Shipman, S.L., and Nicoll, R.A. (2012). A subtype-specific function for the extracellular domain of neuroligin 1 in hippocampal LTP. Neuron *76*, 309–316.

Siddiqui, T.J., Tari, P.K., Connor, S.A., Zhang, P., Dobie, F.A., She, K., Kawabe, H., Wang, Y.T., Brose, N., and Craig, A.M. (2013). An LRRTM4-HSPG complex mediates excitatory synapse development on dentate gyrus granule cells. Neuron *79*, 680–695.

Silverman, J.L., Yang, M., Lord, C., and Crawley, J.N. (2010). Behavioural phenotyping assays for mouse models of autism. Nat. Rev. Neurosci. *11*, 490–502.

Supekar, K., Uddin, L.Q., Khouzam, A., Phillips, J., Gaillard, W.D., Kenworthy, L.E., Yerys, B.E., Vaidya, C.J., and Menon, V. (2013). Brain hyperconnectivity in children with autism and its links to social deficits. Cell Rep. *5*, 738–747.

Takeuchi, A., and O'Leary, D.D. (2006). Radial migration of superficial layer cortical neurons controlled by novel Ig cell adhesion molecule MDGA1. J. Neurosci. *26*, 4460–4464.

Takeuchi, T., Duszkiewicz, A.J., and Morris, R.G. (2013). The synaptic plasticity and memory hypothesis: encoding, storage and persistence. Philos. Trans. R. Soc. Lond. B Biol. Sci. *369*, 20130288.

Tsien, J.Z., Huerta, P.T., and Tonegawa, S. (1996). The essential role of hippocampal CA1 NMDA receptor-dependent synaptic plasticity in spatial memory. Cell *87*, 1327–1338.

Uddin, L.Q., Supekar, K., and Menon, V. (2013). Reconceptualizing functional brain connectivity in autism from a developmental perspective. Front. Hum. Neurosci. *7*, 458.

Wilkerson, J.R., Tsai, N.P., Maksimova, M.A., Wu, H., Cabalo, N.P., Loerwald, K.W., Dictenberg, J.B., Gibson, J.R., and Huber, K.M. (2014). A role for dendritic mGluR5-mediated local translation of Arc/Arg3.1 in MEF2-dependent synapse elimination. Cell Rep. *7*, 1589–1600.

Wills, Z.P., Mandel-Brehm, C., Mardinly, A.R., McCord, A.E., Giger, R.J., and Greenberg, M.E. (2012). The nogo receptor family restricts synapse number in the developing hippocampus. Neuron *73*, 466–481.

Yizhar, O., Fenno, L.E., Prigge, M., Schneider, F., Davidson, T.J., O'Shea, D.J., Sohal, V.S., Goshen, I., Finkelstein, J., Paz, J.T., et al. (2011). Neocortical excitation/inhibition balance in information processing and social dysfunction. Nature *477*, 171–178.

Zhang, Y., Bonnan, A., Bony, G., Ferezou, I., Pietropaolo, S., Ginger, M., Sans, N., Rossier, J., Oostra, B., LeMasson, G., and Frick, A. (2014). Dendritic channelopathies contribute to neocortical and sensory hyperexcitability in Fmr1(-/y) mice. Nat. Neurosci. *17*, 1701–1709.